bioRxiv preprint doi: https://doi.org/10.1101/449553; this version posted October 31, 2018. The copyright holder for this preprint (which was not certified by peer review) is the author/funder, who has granted bioRxiv a license to display the preprint in perpetuity. It is made available under aCC-BY 4.0 International license.

The genome of the plague-resistant great gerbil reveals species-specific duplication of an MHCII gene

Pernille Nilsson[1*], Monica H. Solbakken[1], Boris V. Schmid[1], Russell J. S. Orr[2], Ruichen Lv[3], Yujun Cui[3], Yajun Song[3], Yujiang Zhang[4], Nils Chr. Stenseth[1,5], Ruifu Yang[3], Kjetill S. Jakobsen[1], W. Ryan Easterday[1] & Sissel Jentoft[1]

[1] Centre for Ecological and Evolutionary Synthesis, Department of Biosciences, University of Oslo

[2] Natural History Museum, University of Oslo, Oslo, Norway

[3] State Key Laboratory of Pathogen and Biosecurity, Beijing Institute of Microbiology and Epidemiology, Beijing 100071, China

[4] Xinjiang Center for Disease Control and Prevention, Urumqi, China

[5] Ministry of Education Key Laboratory for Earth System Modeling, Department of Earth System Science, Tsinghua University, Beijing 100084, China

[*] Corresponding author, pernillle.nilsson@ibv.uio.no

Abstract

The great gerbil (*Rhombomys opimus*) is a social rodent living in permanent, complex burrow systems distributed throughout Central Asia, where it serves as the main host of several important vector-borne infectious diseases and is defined as a key reservoir species for plague (*Yersinia pestis*). Studies from the wild have shown that the great gerbil is largely resistant to plague but the genetic basis for resistance is yet to be determined. Here, we present a highly contiguous annotated genome assembly of great gerbil, covering over 96 % of the estimated 2.47 Gb genome. Comparative genomic analyses focusing on the immune

bioRxiv preprint doi: https://doi.org/10.1101/449553; this version posted October 31, 2018. The copyright holder for this preprint (which was not certified by peer review) is the author/funder, who has granted bioRxiv a license to display the preprint in perpetuity. It is made available under aCC-BY 4.0 International license.

gene repertoire, reveal shared gene losses within *TLR* gene families (i.e. *TLR8*, *TLR10* and all members of *TLR11*-subfamily) for the Gerbillinae lineage, accompanied with signs of diversifying selection of *TLR7* and *TLR9*. Most notably, we find a great gerbil-specific duplication of the *MHCII DRB* locus. *In silico* analyses suggest that the duplicated gene provides high peptide binding affinity for *Yersiniae* epitopes. The great gerbil genome provides new insights into the genomic landscape that confers immunological resistance towards plague. The high affinity for *Yersinia* epitopes could be key in our understanding of the high resistance in great gerbils, putatively conferring a faster initiation of the adaptive immune response leading to survival of the infection. Our study demonstrates the power of studying zoonosis in natural hosts through the generation of a genome resource for further comparative and experimental work on plague survival and evolution of host-pathogen interactions.

Main

The great gerbil (*Rhombomys opimus*) is a key plague reservoir species of Central Asia [1] whose habitat stretches from Iran to Kazakhstan to North Eastern China. This diurnal, fossorial rodent lives in arid and semi-arid deserts, and forms small family groups that reside in extensive and complex burrow systems with a large surface diameter and multiple entrances, food storage and nesting chambers [2]. Where great gerbil communities coincide with human settlements and agriculture they are often viewed as pests through the destruction of crops and as carriers of vector-borne diseases [3-5]. Great gerbil is a dominant plague host species in nearly a third of the plague reservoirs located in the vast territories of Russia, Kazakhstan and China [6].

bioRxiv preprint doi: https://doi.org/10.1101/449553; this version posted October 31, 2018. The copyright holder for this preprint (which was not certified by peer review) is the author/funder, who has granted bioRxiv a license to display the preprint in perpetuity. It is made available under aCC-BY 4.0 International license.

Plague, caused by the gram-negative bacterium *Yersinia pestis*, is a common disease in wildlife rodents living in semi-arid deserts and montane steppes, as well as in tropical regions [7,8]. It is predominantly transmitted between rodents by fleas living on rodents or in rodent nests [9] and regularly spills over into human populations [10], leading to individual cases and sometimes localized plague outbreaks [11]. Historically, spillover has resulted in three major human pandemics and continues to cause annual outbreaks of human plague cases in Madagascar [12-14]. Humans have played an important role in spreading the disease globally [15]. However, they are generally dead-end hosts and the long-term persistence of plague depends on plague reservoirs, which are areas where the biotic and abiotic conditions are favoring the bacterium's survival [5].

Most commonly plague enters the body through a subcutaneous flea-bite of an infected flea, being deposited in the dermal tissue of the skin [9,16]. Once the primary physical barriers of the mammalian immune defense have been breached, the pathogen encounters a diverse community of innate immune cells and proteins evolved to recognize and destroy invasive pathogens. Here, Toll-like receptors (TLRs) and other pattern recognition receptors (PRRs) are at the forefront and have a vital role in the recognition and initiation of immune responses. Stimulation of adaptive immunity is in turn governed by the major histocompatibility complex (MHCs). MHC class I (MHCI) and class II (MHCII) proteins present antigens to CD8+ and CD4+ T lymphocytes, respectively. In particular, the CD4+ T lymphocyte is a master activator and regulator of adaptive immune responses [17,18].

In host-pathogen interactions, both sides evolve mechanisms to overpower the other engaging in an evolutionary arms race that shapes the genetic diversity on both sides [19,20].

bioRxiv preprint doi: https://doi.org/10.1101/449553; this version posted October 31, 2018. The copyright holder for this preprint (which was not certified by peer review) is the author/funder, who has granted bioRxiv a license to display the preprint in perpetuity. It is made available under aCC-BY 4.0 International license.

Y. pestis evoke a specialized and complex attack to evade detection and destruction by the mammalian immune system to establish infection [21]. Upon entering a mammalian host, the change in temperature to 37°C initiates a change in bacterial gene expression switching on a wealth of virulence genes whose combined action enables *Y. pestis* to evade both extracellular and intracellular immune defenses [22] at the site of infection, in the lymph node and finally in the colonized blood-rich organs [16,23-26]. The host, in addition to standard immune responses, will have to establish counter measures to overcome the *Y. pestis* strategy of suppressing and delaying the innate immune responses [27,28]. This includes recognition of pathogen, resisting the bacterial signals that induce apoptosis of antigen presenting cells (APCs) and successfully producing an inflammatory response that can overpower the infection while avoiding hyperactivation.

Like all main plague reservoir hosts great gerbils can cope remarkably well with plague infections with only a minor increase in mortality levels compared to the natural mortality (see [10,29] for details). In a laboratory setting, a very large dose of *Y. pestis* is required before a lethal dose is reached where half the injected animals die (LD50) [30]. Variation in plague resistance do exists between individual great gerbils [30] however, the genetic basis of plague resistance and the differences in survival is still unclear. The adaptive immune system requires several days to respond to an infection and *Y. pestis* progresses so rapidly that it can kill susceptible hosts within days. Consequently, the genetic background of the innate immune system could potentially play a pivotal part in plague survival and also contribute to the observed heterogeneity in plague resistance [31]. For a successful response the innate immune system would have to keep the infection in check whilst properly activating the adaptive immune system [18], which can then mount an appropriate

bioRxiv preprint doi: https://doi.org/10.1101/449553; this version posted October 31, 2018. The copyright holder for this preprint (which was not certified by peer review) is the author/funder, who has granted bioRxiv a license to display the preprint in perpetuity. It is made available under aCC-BY 4.0 International license.

96 immune response leading to a more efficient and complete clearance of the pathogen.
97 Previous studies investigating plague resistance have indeed implicated components of both
98 innate [32-38] and adaptive immunity [39,40]. Although, none of these studies have involved
99 wild reservoir hosts in combination with whole-genome sequencing, an approach with
100 increased resolution that can be used in a comparative genomic setting to investigate
101 adaptation, evolution and disease.
102
103 The importance of studying (the genetics/genomics of) zoonosis in their natural hosts is
104 increasingly recognized [41] and the advances in sequencing technology has made it possible
105 and affordable to do whole-genome sequencencing of non-model species for individual and
106 comparative analysis of hosts facing a broad range of zoonosis [41].
107 In this paper, we present a *de novo* whole-genome sequence assembly of the major plague
108 host, the great gerbil. We use this new resource to investigate the genomic landscape of
109 innate and adaptive immunity with focus on candidate genes relevant for plague resistance
110 such as *TLRs* and MHC, through genomic comparative analyses with the closely related
111 plague hosts Mongolian gerbil (*Meriones unguiculatus*) and sand rat (*Psammomys obesus*)
112 and other mammals.
113

114 ## Results

115 ### Genome assembly and annotation

116 We sequenced the genome of a wild-caught male great gerbil, sampled from the Xinjiang
117 Province in China, using the Illumina HiSeq 2000/2500 platform (Additional file 2: Table S1
118 and S2). The genome was assembled *de novo* using ALLPATHS-LG resulting in an assembly
119 consisting of 6,390 scaffolds with an N50 of 3.6 Mb and a total size of 2.376 Gb (Table 1),

bioRxiv preprint doi: https://doi.org/10.1101/449553; this version posted October 31, 2018. The copyright holder for this preprint (which was not certified by peer review) is the author/funder, who has granted bioRxiv a license to display the preprint in perpetuity. It is made available under aCC-BY 4.0 International license.

thus covering 96.4 % of the estimated genome size of 2.47 Gb. Assembly assessment with CEGMA and BUSCO, which investigates the presence and completeness of conserved eukaryotic and vertebrate genes, reported 85.88 % and 87.5 % gene completeness, respectively (Table 1). We were also able to locate all 39 *HOX* genes conserved in four clusters on four separate scaffolds through gene mining (Additional file 1: Fig S1). Further genome assessment with Blobology, characterizing possible contaminations, demonstrated a low degree of contamination, reporting that more than 98.5 % of the reads/bases had top hits of Rodentia. Thus, no scaffolds were filtered from our assembly.

Annotation was performed using the MAKER2 pipeline and resulted in 70 974 predicted gene models of which 22 393 protein coding genes were retained based on default filtering on Annotation Edit Distance score (AED<1).

Table 1. Great gerbil genome assembly statistics.

Assembly metrics	
Total size of scaffolds (bp)	2 376 008 858
Estimated genome size (bp)	2 464 792 293
Number of scaffolds	6 389
Scaffold N50 (bp)	3 610 217
Longest scaffold (bp)	16 185 803
Total size of contigs (bp)	2 216 488 676
Number of contigs	106 018
Contig N50 (bp)	56 880
Assembly validation	
Complete CEGMA[a] genes	85.88 % (213/248)
Partial CEGMA genes	95.16 % (236/248)
Complete Single-copy BUSCOs[b]	2 114 (69.9 %)
Complete duplicated BUSCOs	21 (0.69 %)
Fragmented BUSCOs	533 (17.6 %)
Missing BUSCOs	377 (12.5 %)
Total BUSCOs searched	3 023

[a] Based on 248 highly Conserved Eukaryotic Genes (CEGs), [b] Based on 3,023 vertebrate-specific BUSCO genes

bioRxiv preprint doi: https://doi.org/10.1101/449553; this version posted October 31, 2018. The copyright holder for this preprint (which was not certified by peer review) is the author/funder, who has granted bioRxiv a license to display the preprint in perpetuity. It is made available under aCC-BY 4.0 International license.

Legend: The table details scaffold and contig assembly statistics as well as results from the assembly validation on genic completeness with CEGMA and BUSCO.

Reduced TLR repertoire in great gerbil and Gerbillinae

We characterized the entire *TLR* genetic repertoire in the great gerbil genome and found 13 *TLRs*: *TLR1-13* (Fig. 1). Of these, *TLR1-7* and *TLR9* were complete with signal peptide, ecto-domain, transmembrane domain, linker and Toll/interleukin 1 receptor (TIR) domain that phylogenetically clustered well within each respective subfamily (Table 2 and Fig.2). For the remaining five *TLRs*, we were only able to retrieve fragments of *TLR8* and *TLR10* genes and although sequences of *TLR11-13* were near full length, all three members of the *TLR11* subfamily are putative non-functional pseudogenes as they contain numerous point mutations that creates premature stop codons and frameshift-causing indels. In addition, *TLR12* contains a large deletion of 78 residues (Additional file 1: Figure S2). For *TLR8*, the recovered sequence almost exclusively covers the conserved TIR domain. Relative synteny of *TLR7* and *TLR8* on chromosome X is largely conserved in both human and published rodent genomes, as well as in the great gerbil with the fragments of *TLR8* being located upstream of the full-length sequence of *TLR7* on scaffold00186 (Additional file 1: Figure S3). The great gerbil *TLR10* fragments are located on the same scaffold as full-length *TLR1* and *TLR6* (scaffold00357), in a syntenic structure comparable to other mammals (Additional file 1: Figure S3). In addition to being far from full-length sequences, the pieces of *TLR8* and *TLR10* in the great gerbil genome have point mutations that creates premature stop codons and frameshift-causing indels (Additional file 1: Figure S2). The same *TLR* repertoire is seen in great gerbils' closest relatives, Mongolian gerbil and sand rat, with near full-length sequences of *TLR12* and *TLR13* and shorter fragments of *TLR8* and *TLR10*. Interestingly, for

bioRxiv preprint doi: https://doi.org/10.1101/449553; this version posted October 31, 2018. The copyright holder for this preprint (which was not certified by peer review) is the author/funder, who has granted bioRxiv a license to display the preprint in perpetuity. It is made available under aCC-BY 4.0 International license.

159 *TLR11* only shorter fragments were located for these two species, which is in contrast to the
160 near full-length sequence identified in great gerbil. Moreover, also in these two species
161 premature stop codons and indel-causing frameshifts were present in both the near full-
162 length and fragmented genes (Fig. 1 and Additional file 1: Figure S2).
163

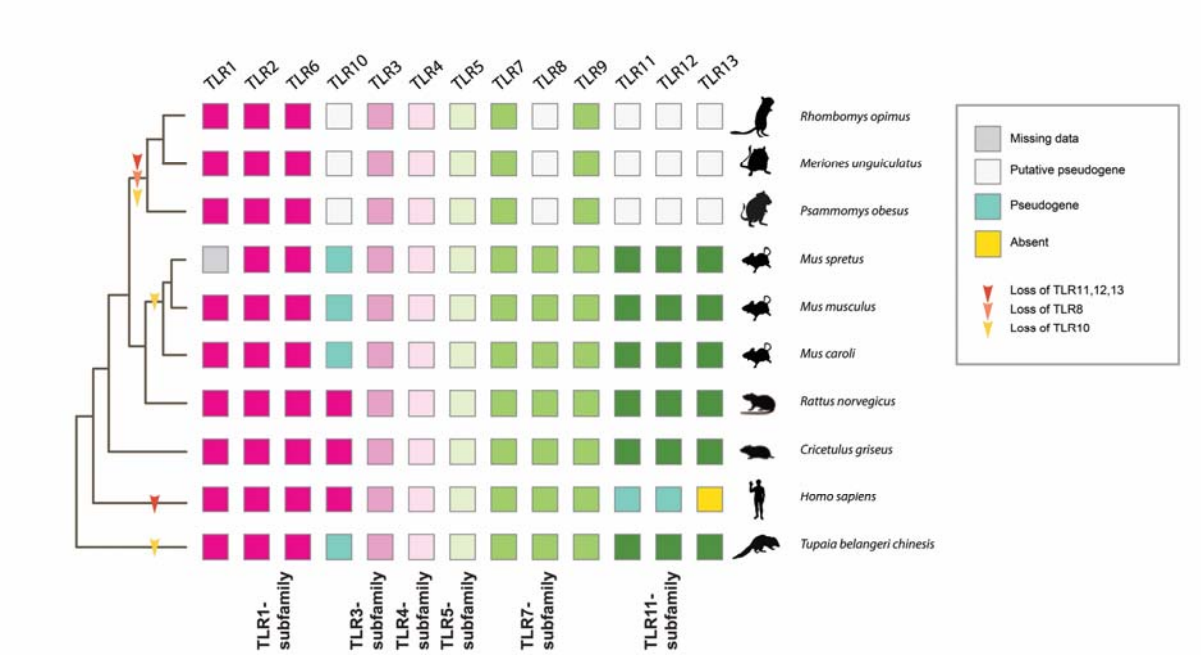

164

165 **FIG. 1 TLR repertoire in Gerbillinae compared to members of Rodentia, human and Chinese**
166 **tree shrew**

167 **FIG. 1** *TLR* repertoire of the investigated Gerbillinae, Rodentia, human and Chinese tree shrew
168 mapped onto a composite cladogram (see Additional file 1: Figure S4). The lineage specific loss of
169 *TLR8* and all members of the *TLR11-subfamily* in Gerbillinae and other lineage-specific *TLR* losses are
170 marked by arrows. Depicted in boxes colored by the six major subfamilies are the individual species'
171 *TLR* repertoires: *TLR1-subfamily* (dark pink), *TLR3-subfamily* (pink), *TLR4-subfamily* (light pink), *TLR5-*
172 *subfamily* (light green), *TLR7-subfamily* (green) and *TLR11-subfamily* (dark green). Teal colored boxes
173 represent established pseudogenes, empty (white) boxes indicate putative pseudogenes, yellow
174 boxes indicate complete absence of genes and grey boxes represent missing information.

bioRxiv preprint doi: https://doi.org/10.1101/449553; this version posted October 31, 2018. The copyright holder for this preprint (which was not certified by peer review) is the author/funder, who has granted bioRxiv a license to display the preprint in perpetuity. It is made available under aCC-BY 4.0 International license.

Table 2. Overview of *TLRs* in great gerbil and their location in the genome assembly.

Gene	Scaffold	Strand	Start	End	Size (aa)	Full-length coding sequence
TLR1	scaffold00357	+	837 967	840 348	794	Yes
TLR2	scaffold00513	+	45 595	47 946	784	Yes
TLR3	scaffold00205	-	1 713 605	1 703 075	905	Yes
TLR4	scaffold00158	+	3 555 106	3 573 424	838	Yes
TLR5	scaffold00165	-	2 379 076	2 376 503	858	Yes
TLR6	scaffold00357	+	820 802	823 186	795	Yes
TLR7	scaffold00186	-	3 421 186[a]	3 418 040	1049	Yes[b]
TLR8	scaffold00186	-			130	No[c]
TLR9	scaffold00044	+	7 083 426[a]	7 086 521	1032	Yes[b]
TLR10	scaffold00357	+			341	No
TLR11	scaffold00001	+			917	Yes[d]
TLR12	scaffold00071	-	4 008 732	4 006 236	817	No[d]
TLR13	scaffold00845	-			899	Yes[d]

[a] Start of second codon in sequence

[b] Missing start codon

[c] Close to complete TIR domain plus c-terminal

[d] Contains multiple point mutations and indels causing frameshifts

Legend: The table details which scaffolds and in what orientation each *TLR* is located as well as coordinates for the start and end of each gene (except for the pseudogenes) on the respective scaffolds. Information on the size of the translated amino acid sequence and whether it is complete is also shown.

bioRxiv preprint doi: https://doi.org/10.1101/449553; this version posted October 31, 2018. The copyright holder for this preprint (which was not certified by peer review) is the author/funder, who has granted bioRxiv a license to display the preprint in perpetuity. It is made available under aCC-BY 4.0 International license.

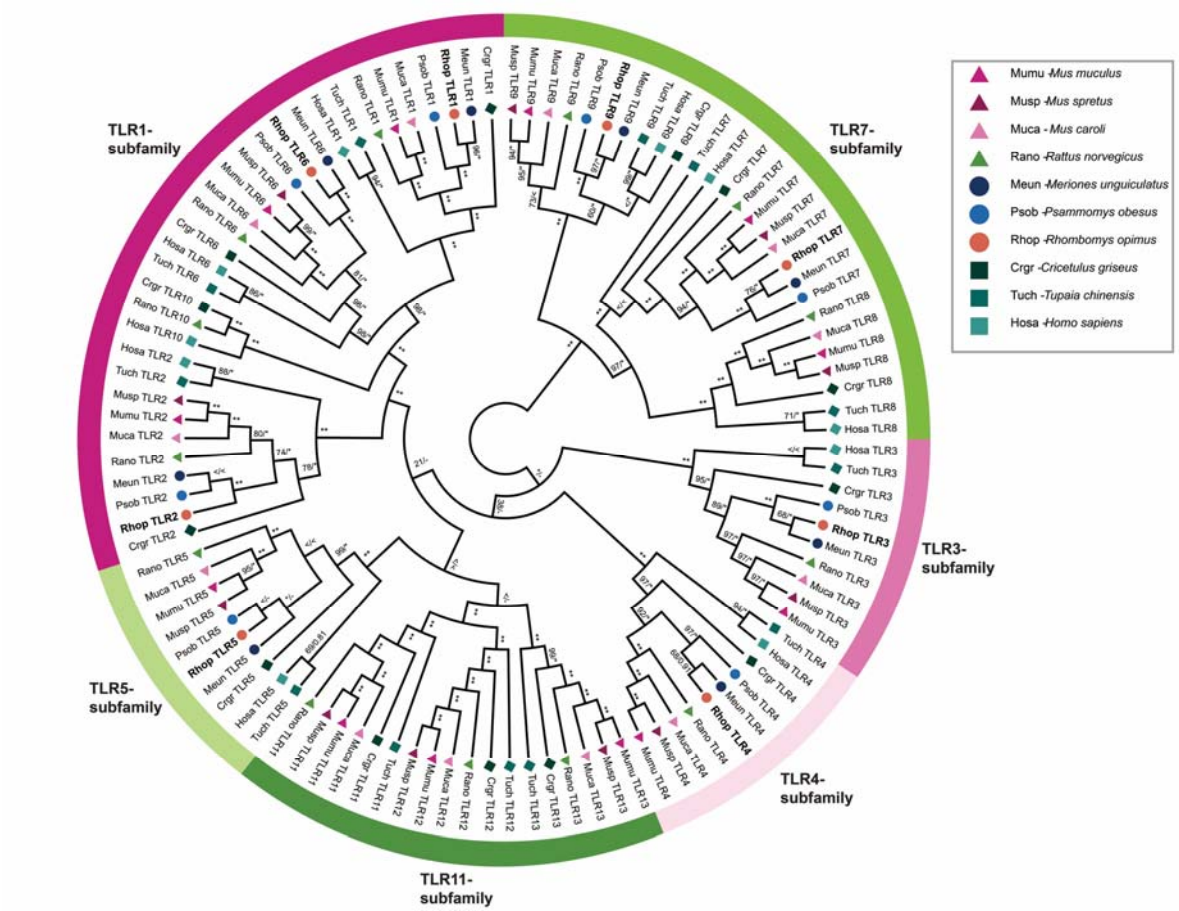

FIG.2 ML-phylogeny of full-length TLRs present in all investigated Gerbillinae, Rodentia, human and Chinese tree shrew

FIG.2 A Maximum likelihood (ML) phylogeny of nucleotide sequences all full-length *TLRs* was created using RAxML with 100x topology and 500x bootstrap replicates. A MrBayes phylogeny with 20,000,000 generations and 25 % burn-in was also created and the posterior probabilities added to the RAxML phylogeny. Great gerbil genes are marked in bold and by orange circles. The six major *TLR* subfamilies are marked with colored bars and corresponding names. All investigated *TLRs* including great gerbil's, cluster well within each subfamily as well as being clearly separated into each *TLR* subfamily member.

Diversifying selection of *TLRs*

bioRxiv preprint doi: https://doi.org/10.1101/449553; this version posted October 31, 2018. The copyright holder for this preprint (which was not certified by peer review) is the author/funder, who has granted bioRxiv a license to display the preprint in perpetuity. It is made available under aCC-BY 4.0 International license.

198 To explore possible variations in selective pressure across the species in our analysis, we ran
199 the adaptive branch-site random effects model (aBSREL) on all full-length *TLRs*. Evidence of
200 episodic positive selection was demonstrated for the Gerbillinae lineage for *TLR7* and *TLR9*
201 and for the Mongolian gerbil *TLR7* specifically (Additional file 1: Figure S5 and S6).
202 Additionally, all full-length great gerbil *TLRs* were analyzed for sites under selection using
203 phylogeny guided mixed effects model of evolution (MEME), from the classic datamonkey
204 and datamonkey version 2.0 websites. Reported sites common between both analyses for all
205 full-length *TLRs* at p-value 0.05 and their distribution among each domain of the proteins are
206 listed in Additional file 2: Table S3. Overall, the sites under selection were almost exclusively
207 located in the ecto-domains with a few sites located in the signal peptide (*TLR3*, *TLR6* and
208 *TLR9*) and in the Linker and TIR domains (*TLR1*, *TLR2*, *TLR4* and *TLR5*). The 3D protein
209 structure of TLR4, TLR7 and TLR9 modelled onto the human TLR5 structure further
210 demonstrated that the sites are predominantly located in loops interspersed between the
211 leucine-rich repeats (Additional file 1: Figures S7-9).
212
213 Scrutiny of the TLR4 amino acid sequence alignment revealed drastic differences in the
214 properties of the residues at two positions reported to be important for maintaining
215 signaling of hypoacetylated lipopolysaccharide (LPS). In rat (*Rattus norvegicus*) and all mouse
216 species used in this study, the residues at position 367 and 434 are basic and positively
217 charged while for the remaining species in the alignment including all Gerbillinae, the
218 residues are acidic and negatively charged.
219

220 **Characterization of the great gerbil class I MHC region**

bioRxiv preprint doi: https://doi.org/10.1101/449553; this version posted October 31, 2018. The copyright holder for this preprint (which was not certified by peer review) is the author/funder, who has granted bioRxiv a license to display the preprint in perpetuity. It is made available under aCC-BY 4.0 International license.

The overall synteny of the MHCI region is well conserved in great gerbil, displaying the same translocation of some *MHCI* genes upstream of the MHCII region as demonstrated in mouse and rat i.e. with a distinct separation of the MHCI region into two clusters (Fig. 3). Some of the great gerbil copies were not included in the phylogeny due to missing data, which hindered their annotation. Additionally, the annotation was obstructed either by the copies being located on scaffolds not containing framework genes or due to variation in the micro-synteny of those particular loci of *MHCIa* and *MHCIb* between mouse, rat and great gerbil (Fig. 3). From the synteny it appears that *MHCI* genes are missing in the region between framework genes *Trim39* and *Trim26* and possibly between *Bat1* and *Pou5f1* in the great gerbil. For full gene names for these and other framework genes mentioned below, see Additional file 2: Table S4.

We were able to identify six scaffolds containing *MHCI* genes (Fig. 3 and Additional file 2: Table S5. Four of the scaffolds contained framework genes that enabled us to orient them. In total, we located 16 *MHCI* copies, of which we were able to obtain all three α domains for 10 of the copies. Three copies contain 2 out of 3 domains while for the last three copies we were only able to locate the α3 domain. In one instance, the missing α domain was due to an assembly gap. Reciprocal BLAST confirmed hits as *MHCI* genes. Due to high similarity between different *MHCI* lineages annotation of identified sequences was done through phylogenetic analyses and synteny. Our phylogeny reveals both inter- and intraspecific clustering of the great gerbil *MHCI* genes with other rodent genes with decent statistical support (i.e. bootstrap and/or posterior probabilities) of the internal branches (Fig. 4). Five great gerbil *MHCI* genes (RhopA1-5) cluster together in a main monophyletic clade while the remaining copies cluster with mouse and rat *MHCIb* genes. Two of the copies (Rhop-A3ψ

bioRxiv preprint doi: https://doi.org/10.1101/449553; this version posted October 31, 2018. The copyright holder for this preprint (which was not certified by peer review) is the author/funder, who has granted bioRxiv a license to display the preprint in perpetuity. It is made available under aCC-BY 4.0 International license.

and Rhop-M6ψ) appear to be pseudogenes as indicated by the presence of point mutations and frameshift-causing indels. Additionally, our phylogeny displays a monophyletic clustering of human *MHCI* genes (Fig. 4). The clade containing five of the great gerbil *MHCI* genes (Rhop-A1-5) possibly include a combination of both classical (*MHCIa*) and non-classical (*MHCIb*) genes as is the case for mouse and rat, where certain *MHCIb* genes cluster closely with *MHCIa* genes (Fig. 3 and Fig. 4). Also, due to the high degree of sequence similarity of rodent *MHCI* genes the phylogenetic relationship between clades containing non-classical M and T *MHCI* genes could not be resolved by sufficient statistical support.

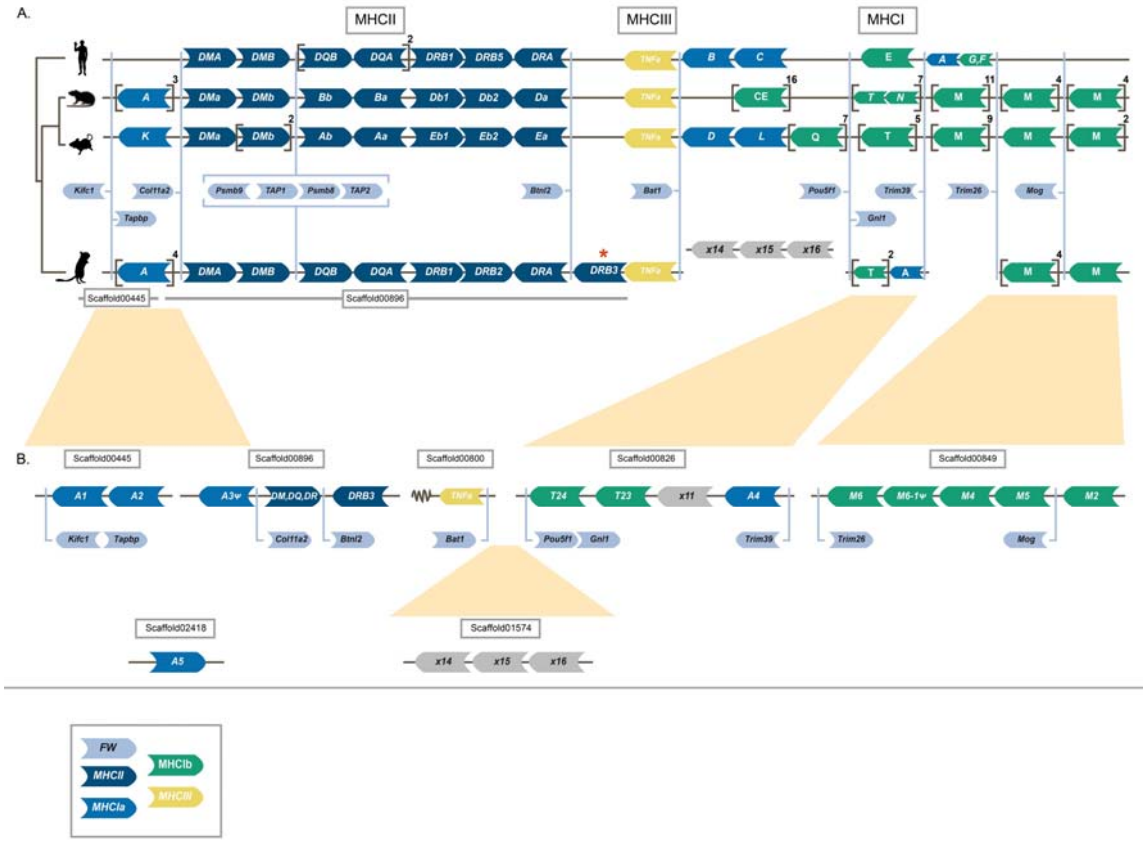

FIG. 3 Synteny of genes in the Major histocompatibility (MHC) region of human, rat, mouse and gerbil

bioRxiv preprint doi: https://doi.org/10.1101/449553; this version posted October 31, 2018. The copyright holder for this preprint (which was not certified by peer review) is the author/funder, who has granted bioRxiv a license to display the preprint in perpetuity. It is made available under aCC-BY 4.0 International license.

FIG 3 Genomic synteny of genes in the MHC regions of human, mouse, rat and great gerbil mapped onto a cladogram. Genes are represented by arrow-shaped boxes indicating the genomic orientation. The boxes are colored by class region and for class I by classical (Ia) or non-classical (Ib) subdivision: Framework (FW) genes (light blue), *MHCII* (dark blue), *MHCIa* (blue), *MHCIII* (yellow) and *MHCIb* (green). Square brackets indicate multiple gene copies not displayed for practical and visualization purposes, but copy number is indicated outside in superscript. Due to limitations in space and to emphasize the conserved synteny of FW genes across lineages, the genes are placed in between the general syntenies and their respective locations are indicated by light blue lines. The light blue brackets surrounding the *Psmb* and *TAP* genes indicates their constitutive organization. Putative pseudogenes are denoted with ψ. For visualization purposes, genes of the *DP* (termed H in rat) and *DO* (termed *O* in mouse) loci are excluded. The location of all great gerbil *MHCII* genes including *Rhop-DP* and *Rhop-DO* can be found in Table 3. (A) Synteny of all MHC regions detailing *MCHI* and *II*. Panel (B) further details the genomic locations of great gerbil *MHCI* genes as indicated by the presence of FW genes located on the scaffolds and inferred from synteny comparisons with human, rat and mouse regions and phylogenetic analysis (see Fig. 4).

The overall synteny of the MHCI and II regions are very well conserved in great gerbil displaying the same translocation of *MHCI* genes upstream of *MHCII* as seen in mouse and rat and resulting in the separation of the MHCI region into two. Most notably, for *MHCII* there is a duplication of a β gene of the *DR* locus in great gerbil (highlighted by a red asterix) whose orientation has changed and is located downstream of the FW gene *Btnl2* that normally represents the end of the MHCII region.

bioRxiv preprint doi: https://doi.org/10.1101/449553; this version posted October 31, 2018. The copyright holder for this preprint (which was not certified by peer review) is the author/funder, who has granted bioRxiv a license to display the preprint in perpetuity. It is made available under aCC-BY 4.0 International license.

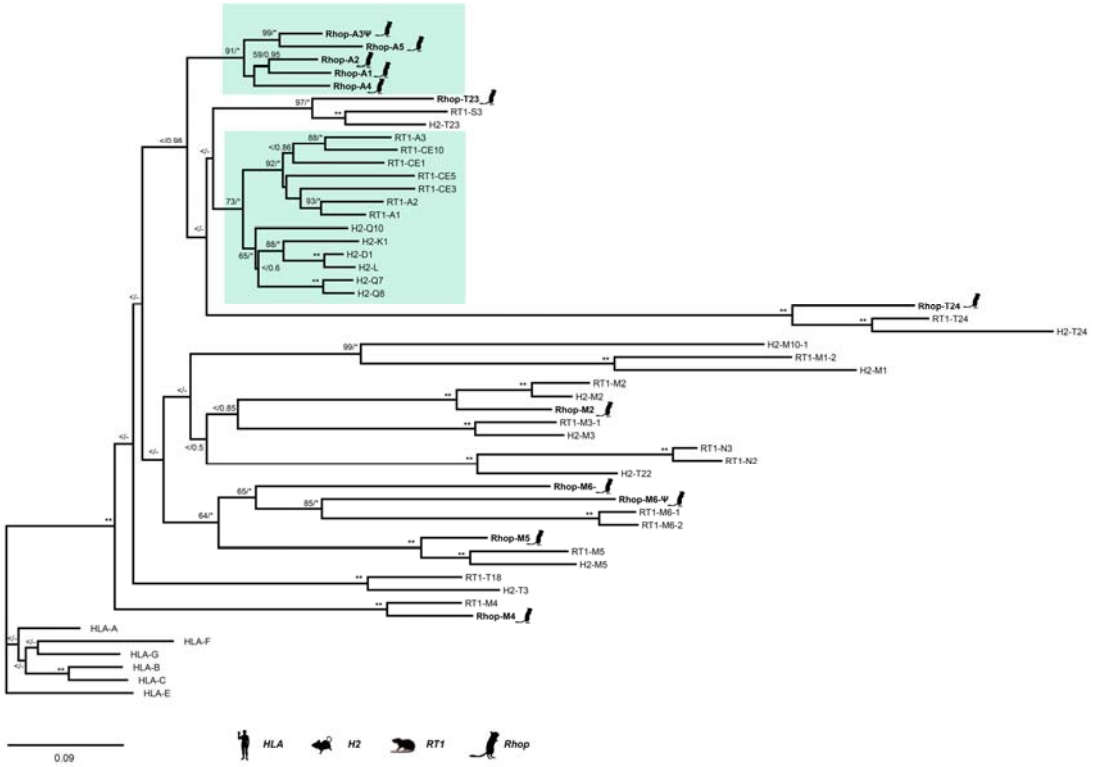

278

279 **FIG. 4 A ML-phylogeny made of nucleotide sequences of the three alpha domains from**

280 **MHCI**

281 **FIG.4** A Maximum likelihood phylogeny of nucleotide sequences containing the three α domains of

282 *MHCI* was created using RAxML with 100x topology and 500x bootstrap replicates. A MrBayes

283 phylogeny with 20,000,000 generations and 25 % burn-in was also created and the posterior

284 probabilities added to the RAxML phylogeny. BS/PP; "*" = BS 100 or PP > 0.96; "**" = BS of 100 and

285 PP>0.97; "<" = support values below 50/0.8 and "-" = node not present in Bayesian analysis. Twelve

286 of the 16 great gerbil sequences were used in the analysis and are marked with a gerbil silhouette

287 and in bold lettering. The remaining four *MHCI* sequences were excluded from the phylogenetic

288 analyses due to missing data exceeding the set threshold of 50 %. The clusters containing *MHCIa*

289 (classical *MHCI*) and the closest related *MHCIb* genes are marked by teal boxes. Putative

290 pseudogenes are denoted with ψ.

291

bioRxiv preprint doi: https://doi.org/10.1101/449553; this version posted October 31, 2018. The copyright holder for this preprint (which was not certified by peer review) is the author/funder, who has granted bioRxiv a license to display the preprint in perpetuity. It is made available under aCC-BY 4.0 International license.

Characterization of the great gerbil class II MHC region

A single scaffold (scaffold00896) of 471 076 bp was identified to contain all genes of the MHCII region, flanked by the reference framework genes *Col11a2* and *Btnl2*. We were able to obtain orthologues of α and β genes of the classical MHCII molecules DP, DQ and DR as well as for the 'non-classical' DM and DO molecules (Table 3). The antigen-processing genes for the class I presentation pathway, *Psmb9*, *TAP1*, *Psmb8* and *TAP2* also maps to scaffold00896 (Fig. 3). Synteny of the MHCII region was largely conserved in great gerbil when compared to mouse, rat and human regions except for a single duplicated copy of *Rhop-DRB* (*Rhop-DRB3*) that was located distal to the *Btnl2* framework gene representing the border between class II and III of the MHC region (Fig. 3). The duplicated copy of the *Rhop-DRB* gene has an antisense orientation in contrast to the other copies of the *Rhop-DRB* genes in great gerbil. In rodents, the DR locus contains a duplication of the β gene and the two copies are termed *β1* and *β2*, with the *β2* gene being less polymorphic than the highly polymorphic *β1* gene. The relative orientation of the β and α genes of the DR locus is conserved in most eutherian mammals studied to date with the genes facing each other, as is the case for Rhop-DRB1, Rhop-DRB2 and Rhop-DRA (Fig. 3). Sequence alignment and a maximum likelihood (ML) phylogeny establishes Rhop-DRB3 to be a duplication of Rhop-DRB1 (Fig. 5). Rhop-DRB1 and Rhop-DRB3 are separated by around 80 kb containing *Rhop-DRB2, Rhop-DRA* and five assembly gaps (Table 3).

Any similar duplication of the *Rhop-DRB1* gene is not seen in either of the two close family members of the Gerbillinae subfamily used in our comparative analyses. BLAST searches of the sand rat genome returned a single full-length copy of the *β1* gene and a near full-length copy of the *β2* gene (Fig. 5 and Additional file 2: Table S6). According to the annotations of

bioRxiv preprint doi: https://doi.org/10.1101/449553; this version posted October 31, 2018. The copyright holder for this preprint (which was not certified by peer review) is the author/funder, who has granted bioRxiv a license to display the preprint in perpetuity. It is made available under aCC-BY 4.0 International license.

316 the Mongolian gerbil genome provided by NCBI, this species contains two copies of the DR
317 locus β genes. A manual tBLASTn search using the protein sequences of Mongolian gerbil
318 *DRB* genes to search the genome assembly did not yield additional hits of β genes in this
319 locus that could have been missed in the automatic annotation process. The phylogeny
320 confirms the copies found in Mongolian gerbil to be $\beta 1$ and $\beta 2$ genes (Fig. 5).
321

322 **Table 3. Overview of great gerbil *MHCII* genes and their location in the genome assembly.**

Gene	Scaffold	Strand	Start	End	Size (aa)	Full-length coding sequence
Rhop-DPB	scaffold00896	-	116 069	105 406	264	Yes
Rhop-DPA	scaffold00896	+	117 514	120 092	252	Yes
Rhop-DOA	scaffold00896	+	125 319	127 406	241	Yes[a]
Rhop-DMa	scaffold00896	+	166 162	168 926	265	Yes[b]
Rhop-DMb	scaffold00896	+	175 763	182 090	257	Yes
Rhop-DOB	scaffold00896	+	239 915	245 006	172	No[c]
Rhop-DQB	scaffold00896	+	271 007	278 482	231	No [d]
Rhop-DQA	scaffold00896	-	294 074	290 301	255	Yes
Rhop-DRB1	scaffold00896	+	310 644	319 368	265	Yes
Rhop-DRB2	scaffold00896	+	326 384	347 931	272	Yes[e]
Rhop-DRA	scaffold00896	-	355 351	351 425	254	Yes
Rhop-DRB3	scaffold00896	-	403 768	395 068	265	Yes

323 [a] Missing final residue and stop codon due to conserved overlapping splice site

324 [b] Unable to locate a stop codon. The structure of the final two exons is conserved among human,
325 mouse and rat with the ultimate residue overlapping the splice site. The final coding exon therefore
326 only contains two bp and the stop codon making it hard to determine the location of the final exon in
327 the gerbil without supporting RNA information.

328 [c] Missing 99 residues (121-219) due to assembly gap

329 [d] Start location is that of exon 2 as exon 1 is missing due to an assembly gap.

330 [e] The cytoplasmic tail of $\beta 2$ genes are encoded by an exon with no known homology to other exons in
331 the MHC II genes and has a low degree of homology between mouse and rat [42]. There is therefore
332 some uncertainty related to the completeness of the final exon of *Rhop-DRB2*.

bioRxiv preprint doi: https://doi.org/10.1101/449553; this version posted October 31, 2018. The copyright holder for this preprint (which was not certified by peer review) is the author/funder, who has granted bioRxiv a license to display the preprint in perpetuity. It is made available under aCC-BY 4.0 International license.

333 Legend: The table details the assigned great gerbil gene names, which scaffold and in what

334 orientation they are located as well as genomic location on the scaffold for start and end of the

335 genes. Information on the size of the translated amino acid sequence and whether it is complete is

336 also shown.

337

bioRxiv preprint doi: https://doi.org/10.1101/449553; this version posted October 31, 2018. The copyright holder for this preprint (which was not certified by peer review) is the author/funder, who has granted bioRxiv a license to display the preprint in perpetuity. It is made available under aCC-BY 4.0 International license.

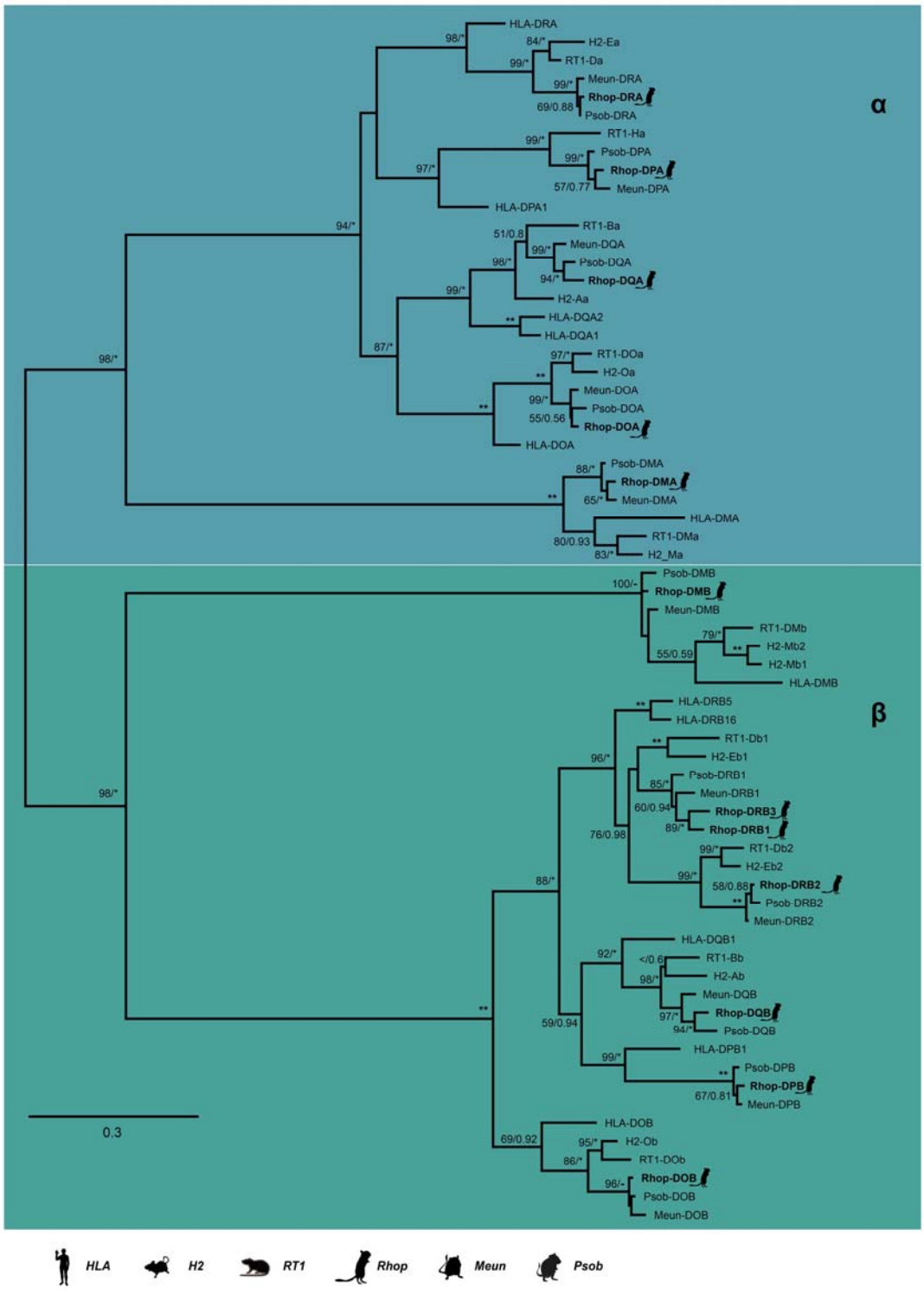

338

339 **FIG. 5 A ML-phylogeny made of nucleotide sequences of domains only from MHCII α and β**

340 **genes**

bioRxiv preprint doi: https://doi.org/10.1101/449553; this version posted October 31, 2018. The copyright holder for this preprint (which was not certified by peer review) is the author/funder, who has granted bioRxiv a license to display the preprint in perpetuity. It is made available under aCC-BY 4.0 International license.

FIG.5 A Maximum likelihood phylogeny of nucleotide sequences containing the α and β domains of *MHCII* α and β genes was created using RAxML with 100x topology and 500x bootstrap replicates. A MrBayes phylogeny with 20,000,000 generations and 25 % burn-in was also created and the posterior probabilities added to the RAxML phylogeny. BS/PP; "*" = BS 100 or PP > 0.96; "**" = BS of 100 and PP>0.97; "<" = support values below 50/0.8 and "-" = node not present in Bayesian analysis. Great gerbil genes are indicated with bold lettering and by silhouettes. The 12 great gerbil *MHCII* genes located in the genome assembly cluster accordingly with the orthologues of human, mouse, rat, sand rat and Mongolian gerbil. The *Rhop-DRB* duplication (*Rhop-DRB3*) cluster closely with the *Rhop-DRB1* and other *DRB1* orthologs with good support. The nomenclature of *MHCII* genes in Gerbillinae are in concordance with the recommendations of the MHC Nomenclature report [43].

MHCII DRB promoters

MHCII genes each contain a proximal promoter with conserved elements (S-X-Y motifs) that are crucial for the efficient expression of the gene. We aligned the proximal promoter of the β genes of the DR locus in great gerbil and the other investigated species to establish if the integrity of the promoter was conserved as well as examining similarities and potential dissimilarities causing the previously reported differences in transcription and expression of $\beta1$ and $\beta2$ genes in rodents [42,44]. The alignment of the promoter region reveals the conserved structure and similarities within $\beta1$ and $\beta2$ genes as well as characteristic differences (Fig. 6 and Table 4). Clear similarities are seen for the proximal promoter regions of *Rhop-DRB1* and *Rhop-DRB3* to the other rodent and human $\beta1$ promoters, as illustrated by high sequence similarity and the presence of a CCAAT box just downstream of the Y motif in all investigated rodent $\beta1$ promoters. Notably, the CCAAT box is missing in $\beta2$ promoters. The crucial distance between the S and X motifs is conserved in all β genes and the integrity of the S-X-Y motifs is observable for *Rhop-DRB1* and *DRB3* promoters. However, both the S

bioRxiv preprint doi: https://doi.org/10.1101/449553; this version posted October 31, 2018. The copyright holder for this preprint (which was not certified by peer review) is the author/funder, who has granted bioRxiv a license to display the preprint in perpetuity. It is made available under aCC-BY 4.0 International license.

366 and X box of *DRB2* are compromised by deletions in great gerbil. The deletion in the X box
367 severely disrupt the motif and reduce its size by half. An identical deletion in the X box is
368 seen in Mongolian gerbil while the sand rat X box sequence covering the deleted parts is
369 highly divergent from the conserved sequence found in the rest of the promoters (Fig. 6).
370 Furthermore, for the *β2* genes, two deletions downstream of the motifs are shared among
371 all rodents in the alignment as well as an additional insertion observed in Gerbillinae
372 members.
373

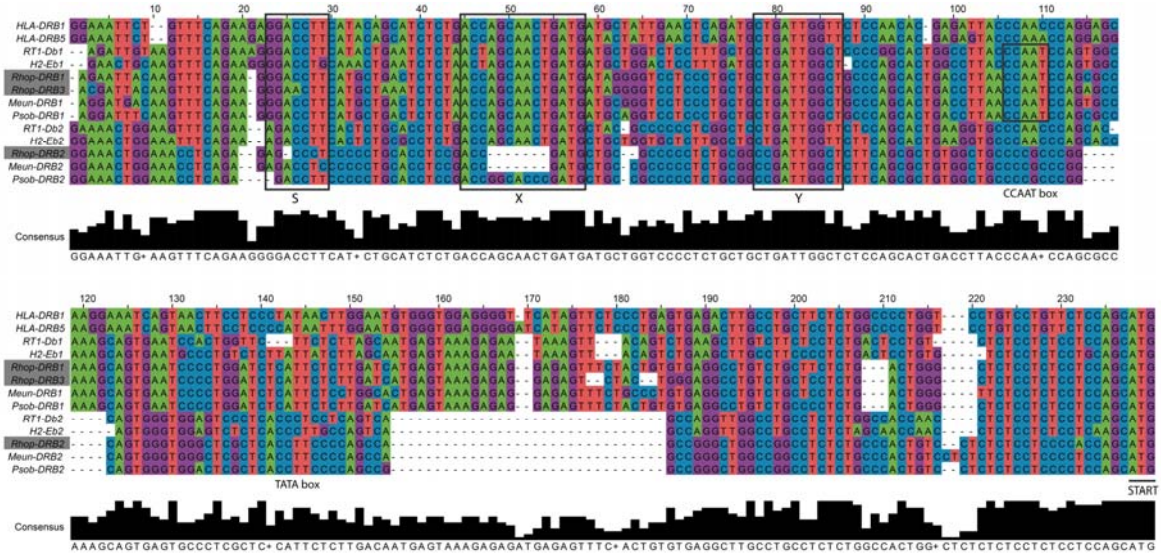

374

375 **FIG. 6 Alignment of the DR locus β1 and β2 proximal promoters**

376 **FIG. 6** Sequences of the proximal promoters of *β1* and *β2* genes of the DR locus (E locus in mouse
377 and D locus in rat) were aligned in MEGA7 [45] using MUSCLE with default parameters. The resulting
378 alignment was edited manually for obvious misalignments and transferred and displayed in Jalview
379 [46]. For visualization purposes only, the alignment was further edited in Adobe Illustrator (CS6),
380 changing colors of the bases and adding boxes to point out the S-X-Y motifs. The three copies of *DRB*
381 genes located in the great gerbil genome are marked with grey boxes. The alignment shows clear
382 similarities of the proximal promoter region of *Rhop-DRB1* and *Rhop-DRB3* to the other rodent and

bioRxiv preprint doi: https://doi.org/10.1101/449553; this version posted October 31, 2018. The copyright holder for this preprint (which was not certified by peer review) is the author/funder, who has granted bioRxiv a license to display the preprint in perpetuity. It is made available under aCC-BY 4.0 International license.

383 human *β1* promoter sequences. For the *DRB2* genes, two deletions are shared among all rodents in
384 the alignment as well as additional indels observed in Gerbillinae members. Most notably, both great
385 gerbil and Mongolian gerbil have deletions of half the X box while sand rat X box sequences in that
386 same position is highly divergent from the otherwise conserved sequence seen in the alignment.
387
388 **Table 4. Coordinates of *MHCII* S-X-Y motifs of the promoters of the *DRB* genes in**
389 **investigated species.**

Gene	S-X spacing (bp)	X-Y spacing (bp)	S-X-Y Relative position (S-X-Y end to gene start)	CCAAT box
HLA-DRB1	15	19	-145	TATA box
HLA-DRB5	15	19	-146	
RT1-Db1	15	19	-137	Yes
H2-Eb1	15	19	-139	Yes + TATA box
Rhop-DRB1	15	19	-141	Yes
Rhop-DRB3	15	19	-137	Yes
Meun-DRB1	15	19	-141	Yes
Psob-DRB1	15	19	-141	Yes
RT1-Db2	15	18	-110	
H2-Eb2	15	19	-110	
Rhop-DRB2	15	17	-109	
Meun-DRB2	15	18	-111	
Psob-DRB2	15	18	-109	

390 Legend: The overview details the relative coordinates for conserved motifs in the promoter regions
391 of great gerbil (*Rhop-DRB*), sand rat (*Psob-DRB*), Mongolian gerbil (*Meun-DRB*), human (*HLA-DRB*),
392 mouse (*H2-Eb*) and rat (*RT1-Db*) orthologous genes. The S-X and X-Y spacing refers to the distance
393 between the S and X, and X and Y motifs, respectively. The S-X-Y Relative position show the distance
394 (bp) between the end of the Y motif and the start codon of the gene.
395
396 **Peptide binding affinity predictions and expression of Rhop-DR MHCII**
397 **molecules**

bioRxiv preprint doi: https://doi.org/10.1101/449553; this version posted October 31, 2018. The copyright holder for this preprint (which was not certified by peer review) is the author/funder, who has granted bioRxiv a license to display the preprint in perpetuity. It is made available under aCC-BY 4.0 International license.

Mouse and rat β2 molecules have been shown to have an extraordinary capacity to present the *Y. pseudotuberculosis* superantigen mitogen (YPm) [42]. We therefore investigated the peptide binding affinities of the Rhop-DR molecules by running translations of *Rhop-DRA* in combinations with each of the three *Rhop-DRB* genes through the NetMHCIIpan 3.2 server [47] along with peptide/protein sequences of YPm, *Y. pestis* F1 'capsular' antigen and LcrV antigen. Universally, the Rhop-DRB3 shows an affinity profile identical to that of Rhop-DRB2 displaying high affinity towards both *Y. pseudotuberculosis* and *Y. pestis* epitopes while Rhop-DRB1 does not (Fig.7 and Additional file 3). The translated great gerbil MHCII from DP and DQ loci were also tested for peptide binding affinity but only Rhop-DP displayed affinity to one of the epitopes tested. Furthermore, analyses of the translated amino acid sequences of sand rat DR (Psob-DR) molecules as well as published protein sequences of Mongolian gerbil DR (Meun-DR) molecules and the mouse ortholog H2-E confirmed the high affinity of β2 molecules to *Y. pseudotuberculosis* and *Y. pestis* (Additional file 1: Figure S10 and Additional file 3). The equal capacity of Rhop-DRB2 and Rhop-DRB3 to putatively present *Yersiniae* combined with the proximal promoter investigations lead us to question the expression of DRB genes in great gerbil. Searching a set of raw counts of great gerbil expressed genes, reveal that Rhop-DRB1 and Rhop-DRB3 are both similarly expressed at similar levels while Rhop-DRB2 is not expressed or at undetectable levels (3936 and 2279 vs 14).

bioRxiv preprint doi: https://doi.org/10.1101/449553; this version posted October 31, 2018. The copyright holder for this preprint (which was not certified by peer review) is the author/funder, who has granted bioRxiv a license to display the preprint in perpetuity. It is made available under aCC-BY 4.0 International license.

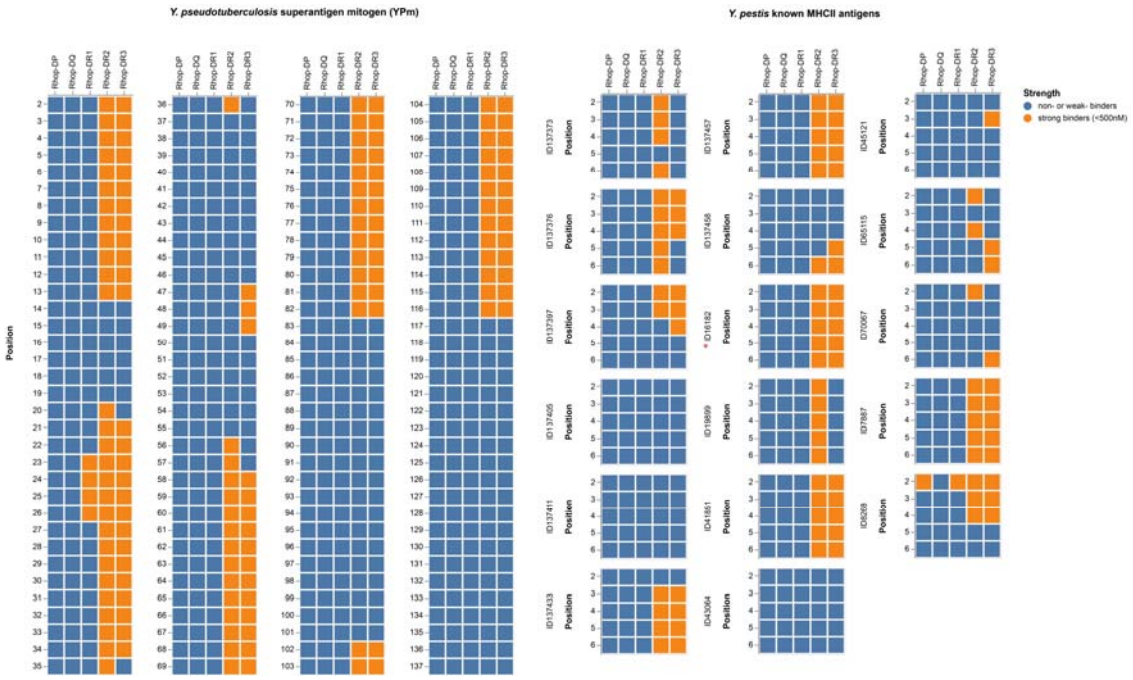

418

419 **Figure 7 Affinity predictions of great gerbil MHCII molecules**

420 **FIG. 7** Affinity predictions of great gerbil MHC class II molecules represented as a heatmap.

421 For the known *Y. pestis* antigens all are from the F1 capsule precursor except ID16182 (red asterix)

422 which is from the V antigen. Strong binders are defined as <500 nM and depicted in orange, while

423 weak or non-binders are represented in blue.

424

425 ## Discussion

426 Here we present a highly contiguous *de novo* genome assembly of the great gerbil covering

427 over 96 % of the estimated genome size and almost 88 % of the gene space, which is

428 equivalent to the genic completeness reported in the recently published and close relative

429 sand rat genome [48] (Additional file 2: Table S7). By comparative genomic analyses where

430 we include genome data from its close relatives within the Gerbillinae, we provide novel

431 insight into the innate and adaptive immunological genomic landscape of this key plague

432 host species.

bioRxiv preprint doi: https://doi.org/10.1101/449553; this version posted October 31, 2018. The copyright holder for this preprint (which was not certified by peer review) is the author/funder, who has granted bioRxiv a license to display the preprint in perpetuity. It is made available under aCC-BY 4.0 International license.

433

434 ## The *TLR* repertoire in the great gerbil and Gerbillinae

435 *TLRs* are essential components of PRRs and the innate immune system as they alert the
436 adaptive immune system of the presence of invading pathogens [49]. The detailed
437 characterization of *TLRs* did not uncover any species-specific features for the great gerbil.
438 However, a shared *TLR* gene repertoire for the Gerbillinae lineage (i.e. the great gerbil, sand
439 rat and Mongolian gerbil), with gene losses of *TLR8*, *TLR10* and all members of the *TLR11*-
440 subfamily was revealed. This finding could indicate quite similar selective pressures on these
441 species, at least in regard to their function of *TLRs*, all being desert dwelling, burrowing
442 rodents living in arid or semi-arid ecosystems and being capable of carrying plague. Thus, it
443 is possible that the members of this clade have reduced the *TLR* repertoire in a cost-benefit
444 response to environmental constraints or due to altered repertoire of pathogen exposure
445 [50]. These results are in line with the fairly conserved *TLR* gene repertoire reported within
446 the vertebrate lineage [51], although the repertoire of *TLR* genes present within vertebrate
447 groups can show major differences [51-53], presumably in response to presence or lack of
448 certain pathogen or environmental pressures [54,55]. Outside of Gerbillinae, the presence of
449 TLR11-subfamily appears to be universal in Rodentia, however functionally lost from the
450 human repertoire [51,53]. The TLR11-subfamily recognizes parasites and bacteria through
451 profilin, flagellin and 23S ribosomal RNA [56,57] and it is possible that cross-recognition of
452 these patterns by other TLR members or other PRRs might have made the TLR11-subfamily
453 redundant in Gerbillinae and humans [50]. The varying degree of point mutations,
454 frameshift-causing indels and in some cases almost complete elimination of sequence in
455 *TLR8*, *TLR10* and *TLR11-13* in Gerbillinae suggest successive losses of these receptors, where
456 a shared pseudogenization of *TLR12-13* across all species investigated were recorded. For

bioRxiv preprint doi: https://doi.org/10.1101/449553; this version posted October 31, 2018. The copyright holder for this preprint (which was not certified by peer review) is the author/funder, who has granted bioRxiv a license to display the preprint in perpetuity. It is made available under aCC-BY 4.0 International license.

457 *TLR11* however, the pseudogenization seems to have occurred in multiple steps, i.e. with a
458 more recent event in the great gerbil where a near full-length sequence was identified
459 compared to the shorter fragments identified for Mongolian gerbil and sand rat (Additional
460 file 1: Figure S2C). Furthermore, the high degree of shared disruptive mutations among all
461 three species of Gerbillinae indicates that the initiation of pseudogenization predates the
462 speciation estimated to have occurred about 5.5 Mya [58].
463
464 In the context of plague susceptibility, the branch specific diversifying selection reported
465 here for *TLR7* and *TLR9* in Gerbillinae is intriguing, as both receptors have been implicated to
466 affect the outcome of plague infection in mice and humans [59-61]. For instance, the study
467 by Dhariwala et al. (2017) showed, in a murine model, that TLR7 recognizes intracellular *Y.*
468 *pestis* and is important for defense against disease in the lungs but was detrimental to
469 septicemic plague [59]. Moreover, recognition of *Y. pestis* by TLR9 was also demonstrated by
470 Saikh et al. (2009) in human monocytes [61]. All but one of the residues under site specific
471 selection seen in *TLR7* and *TLR9* were located in the ectodomain, which may suggest
472 possible alterations in ligand recognition driven by selection pressure from *Y. pestis* or other
473 shared pathogens. Stimulation of *TLR7* and *TLR9* have also been reported to regulate antigen
474 presentation by *MHCII* in murine macrophages [62]. These data could therefore indicate a
475 possible connection of the selection in *TLR7* and *TLR9* with the great gerbil duplication in
476 *MHCII*. For *TLR4*, the selection tests and sequence alignment analysis did not reveal any
477 branch-specific selection for great gerbil nor Gerbillinae, whereas we did detect signs of site-
478 specific selection in the ectodomain that occasionally was driven by great gerbil or
479 Gerbillinae substitutions. TLR4 is the prototypical PRR for detection of lipopolysaccharides
480 (LPS) found in the outer membrane of gram-negative bacteria like *Y. pestis*. As part of the

bioRxiv preprint doi: https://doi.org/10.1101/449553; this version posted October 31, 2018. The copyright holder for this preprint (which was not certified by peer review) is the author/funder, who has granted bioRxiv a license to display the preprint in perpetuity. It is made available under aCC-BY 4.0 International license.

481 arms race, however, it is well known that gram-negative bacteria, including *Y. pestis*, alter
482 the conformation of their LPS in order to avoid recognition and strong stimulation of the
483 TLR4-MD2-CD14 receptor complex [63-65]. Despite this, in mice at least, some inflammatory
484 signaling still occurs through this receptor complex but require particular residues in TLR4
485 not found to be conserved in the Gerbillinae lineage. Whether other mutations in TLR4 in
486 Gerbillinae have a similar functionality as the residues that allow mice to respond to *Y. pestis*
487 LPS is not known. However, if such functionality is missing in Gerbillinae, the loss of
488 responsiveness to the hypoacetylated LPS [19] could perhaps defer some protection from
489 pathologies caused by excessive initiation of inflammatory responses [66], and thus TLR4 is
490 not likely directly involved in the resistance of plague in great gerbils.
491
492 Cumulatively, our investigations of the great gerbil innate immune system, focusing on the
493 *TLR* gene repertoire, reveal shared gene losses within *TLR* gene families for the Gerbillinae
494 lineage, all being desert dwelling species capable of carrying plague. The evolutionary
495 analyses conducted did not uncover any great gerbil-specific features that could explain
496 their resistance to *Y. pestis*, indicating that other PRRs (not investigated here) could be more
497 directly involved during the innate immune response to plague infection in the great gerbil
498 [36].
499
500 **Great gerbil MHC repertoires**
501 MHCI and II proteins are crucial links between the innate and adaptive immune system
502 continuously presenting peptides on the cell surface for recognition by CD8+ and CD4+ T
503 cells respectively, and MHC genes readily undergo duplications, deletions and
504 pseudogenization [67]. For *MHCI*, the discovery of 16 copies in great gerbil is in somewhat

bioRxiv preprint doi: https://doi.org/10.1101/449553; this version posted October 31, 2018. The copyright holder for this preprint (which was not certified by peer review) is the author/funder, who has granted bioRxiv a license to display the preprint in perpetuity. It is made available under aCC-BY 4.0 International license.

agreement with what has earlier been reported in rodents, where the MHCI region is found to have undergone extensive duplication followed by sub- and neofunctionalization with several genes involved in non-immune functions [68,69]. However, it should be noted that our copy number estimation is most likely an underestimation, due to the assembly collapse in almost all *MHCI* containing regions identified. Furthermore, not all copies could be confidently placed in the gene maps as some scaffolds lacked colocalizing framework genes. These two factors are the probable reason why the great gerbil appears to be lacking some *MHCI* genes compared to mouse and rat.

For *MHCII* we discovered a gerbil-specific duplication that is not present in other closely related plague hosts or in other rodents investigated. The phylogeny established the duplication's (*Rhop-DRB3*) relationship to *Rhop-DRB1* and other mammalian *β1* genes and reflects the orthology of mammalian *MHCII* genes [70]. The localization of *Rhop-DRB3* outside of the generally conserved framework of the *MHCII* region and not in tandem with the other *β* genes of the *DR* locus is unusual and is not generally seen for eutherian mammals. For instance, major duplication events with altered organization and orientation of *DR* and *DQ* genes has been reported for the *MHCII* region in horse (*Equus caballus*), however all genes are found within the framework genes [71]. Duplications tend to disperse in the genome as they age [72], thus the reversed orientation and translocation of the great gerbil copy might indicate that the duplication event is ancient occurring sometime after the species split approximately 5 Mya. However, it must also be noted that there are several assembly gaps located between *Rhop-DRB1* and *Rhop-DRB3* resulting in the possibility of the translocation being a result of an assembly error.

bioRxiv preprint doi: https://doi.org/10.1101/449553; this version posted October 31, 2018. The copyright holder for this preprint (which was not certified by peer review) is the author/funder, who has granted bioRxiv a license to display the preprint in perpetuity. It is made available under aCC-BY 4.0 International license.

529 Predictions of the affinity of the β1, β2 and β3 MHCII molecules to *Y. pestis* and *Y.*
530 *pseudotuberculosis* antigens matched the reported high affinity of rodent β2 molecules for
531 *Yersiniae* epitopes [42]. Rhop-DRB3 had an equally high affinity and largely identical affinity-
532 profile as Rhop-DRB2. A high affinity for *Y. pestis* epitopes is important in the immune
533 response against plague, as the initiation of a T cell response is more efficient and requires
534 fewer APCs and T cells when high-affinity peptides are presented by MHCII molecules [73].
535 In the early stages of an infection where presence of antigen is low, there will be fewer
536 MHCII molecules presenting peptides and affinity for those peptides is paramount to fast
537 initiation of the immune response against the pathogen. Individuals presenting MHCII
538 molecules with high affinity for pathogen epitopes are able to raise an immune defense
539 more quickly and have a better chance of fighting off the rapidly progressing infection than
540 individuals that are fractionally slower. This fractional advantage could mean the difference
541 between death or survival.
542
543 We find comparable expression levels for *Rhop-DRB1* and *Rhop-DRB3* but no detectable
544 expression of *Rhop-DRB2*. These similarities and differences are likely explained by the
545 variations discovered in the proximal promoter of the genes. Integrity of the conserved
546 motifs and the spacing between them is necessary for assembly of the enhanceosome
547 complex of transcription factors and subsequent binding of Class II Major Histocompatibilty
548 Complex transactivator (*CIITA*), and is essential for efficient expression of *MHCII* genes. The
549 conservation of the proximal promoter of *Rhop-DRB3* along with the overall sequence
550 similarity with other *β1* genes are indicative of a similar expression pattern. In contrast, the
551 deletion in the X box of *Rhop-DRB2* reducing the motif to half the size will likely affect the
552 ability of the transcription factors to bind and could explain the lack of expression. Similar

bioRxiv preprint doi: https://doi.org/10.1101/449553; this version posted October 31, 2018. The copyright holder for this preprint (which was not certified by peer review) is the author/funder, who has granted bioRxiv a license to display the preprint in perpetuity. It is made available under aCC-BY 4.0 International license.

553 disruptions in the *β2* genes of the other Gerbillinae were found along with a major deletion
554 further downstream in all *β2* genes that perhaps explains the previously reported low and
555 unusual pattern of transcription for rodent *β2* genes [42,44]. The equal affinity profile but
556 different expression levels of *Rhop-DRB2* and *Rhop-DRB3* could mean that *Rhop-DRB3* has
557 taken over the immune function lost by the lack of expression of *Rhop-DRB2*. The selective
558 pressure might have come from *Yersinia* or pathogens similar to *Yersiniae*. A nonclassical
559 function of MHCII molecules have also been reported where intracellular MHCII interacted
560 with components of the TLR signaling pathway in a way that suggested MHCII molecules are
561 required for full activation of the TLR-triggered innate immune response [74]. Moreover, in
562 vertebrates the *MHCII DRB* genes are identified as highly polymorphic and specific allele
563 variants have frequently been linked to increased susceptibility to diseases in humans [75].
564 Intriguingly, in a recent study by Cobble et al. (2016) it was suggested that allelic variation of
565 the *DRB1* locus could be linked to plague survival in Gunnison's prairie dog colonies [40].
566 Thus, investigating how the genetic variation of the *DRB1* and *DRB3* loci in great gerbil
567 manifests at the population level and the affinity of these allelic variants to *Yersiniae*
568 epitopes, would be the next step to further our understanding of the plague resistant key
569 host species in Central Asia.
570
571 From the analyses conducted on the genomic landscape of the adaptive immune system of
572 the great gerbil, i.e. *MHCI* and *MHCII* more specifically, the most interesting reporting is the
573 duplication of an *MHCII* gene. *In silico* analyses of *Rhop-DRB3* indicate a high predicted
574 affinity for *Y. pestis* epitopes, which may result in faster initiation of the adaptive immune
575 system in great gerbils when exposed to the pathogen, and thus could explain the high
576 degree of plague resistance in this species.

bioRxiv preprint doi: https://doi.org/10.1101/449553; this version posted October 31, 2018. The copyright holder for this preprint (which was not certified by peer review) is the author/funder, who has granted bioRxiv a license to display the preprint in perpetuity. It is made available under aCC-BY 4.0 International license.

Conclusion

Plague has historically had a vast impact on human society through major pandemics, however it mainly circulates in rodent communities. A key issue is to understand host-pathogen interactions in these rodent hosts. From the pathogen-perspective, research has studied how *Y. pestis* has evolved to evade both detection and destruction by the mammalian immune system to establish infection. In this study, we have demonstrated the power of using whole genome sequencing of a wild plague reservoir species to gain new insight into the genomic landscape of its resistance by immuno-comparative analyses with closely related plague hosts and other mammals. We reveal the duplication of an MHCII gene in great gerbils with a computed peptide binding profile that putatively would cause a faster initiation of the adaptive immune system when exposed to *Yersiniae* epitopes. We also find signs of positive selection in *TLR7* and *TLR9*, which have been shown to regulate antigen presentation and impact the outcome of a plague infection. Investigations into how the genetic variation of the MHCII locus manifests at the population level are necessary to further understand the role of the gene duplication in the resistance of plague in great gerbils. Comprehending the genetic basis for plague resistance is crucial to understand the persistence of plague in large regions of the world and the great gerbil *de novo* genome assembly is a valuable anchor for such work, as well as a resource for future comparative work in host-pathogen interactions, evolution (of resistance) and adaptation.

Methods

Sampling and sequencing

bioRxiv preprint doi: https://doi.org/10.1101/449553; this version posted October 31, 2018. The copyright holder for this preprint (which was not certified by peer review) is the author/funder, who has granted bioRxiv a license to display the preprint in perpetuity. It is made available under aCC-BY 4.0 International license.

A male great gerbil weighing 180g was captured in the Midong District outside Urumqi in Xinjiang Province, China in October 2013. The animal was humanely euthanized and tissue samples of liver were conserved in ethanol prior to DNA extraction. Blood samples from the individual were screened for F1 'capsular' antigen (Caf1) and anti-F1 as described in [30,76] to confirm plague negative status. The DNA used in the library construction was extracted from liver tissue using Gentra Puregene Tissue Kit (Qiagen Inc. USA). Use of great gerbil tissue was approved by the Committee for Animal Welfares of Xinjiang CDC, China.

The sequence strategy was tailored towards the ALLPATHS-LG assembly software (Broad Institute, Cambridge, MA) following their recommendations for platform choice and fragment size resulting in the combination of one short paired-end (PE) library with an average insert size of 220 bp (150 bp read length) and two mate-pair (MP) libraries of 3 kbp and 10 kbp insert size (100 bp read length). See Additional file 2: Table S1 for a list of libraries and sequence yields. Sequencing for the *de novo* assembly of the great gerbil reference genome was performed on the Illumina platform using HiSeq2500 instruments at the Norwegian Sequencing Centre at the University of Oslo for the PE library (https://www.sequencing.uio.no) and using HiSeq2000 instruments at Génome Québec at McGill University for the MP libraries (http://gqinnovationcenter.com/index.aspx?l=e).

Genome assembly and Maker annotation

The Illumina sequences were quality checked using FastQC v0.11.2 and SGA-preqc (downloaded 25th June 2014) with default parameters. Both MP libraries were trimmed for adapter sequences using cutadapt v1.5 with option -b and a list of adapters used in MP library prep [77] and the trimmed reads were used alongside the PE short read as input for

bioRxiv preprint doi: https://doi.org/10.1101/449553; this version posted October 31, 2018. The copyright holder for this preprint (which was not certified by peer review) is the author/funder, who has granted bioRxiv a license to display the preprint in perpetuity. It is made available under aCC-BY 4.0 International license.

624 ALLPATHS-LG v48639 generating a *de novo* assembly. This combination of short-read
625 sequencing technology combined with the ALLPATHS-LG assembly algorithm is documented
626 to perform well in birds and mammals [78-80]. File preparations were conducted according
627 to manufacturer's recommendation and the option TARGETS=submission was added to the
628 run to obtain a submission prepared assembly version.
629
630 Assembly completeness was assessed by analysing the extent of conserved eukaryotic genes
631 present using CEGMA v2.4.010312 and BUSCO v1.1.b [81-83]. Gene mining for the highly
632 conserved Homeobox (*HOX*) genes was also conducted as an additional assessment of
633 assembly completeness (see Additional file 1: Note S1 and Figure S10).
634 All reads were mapped back to the assembly using BWA-MEM v 0.7.5a and the resulting
635 bam files were used alongside the assembly in REAPR v 1.0.17 to evaluate potential
636 scaffolding errors as well as in Blobology to inspect the assembly for possible contaminants,
637 creating Taxon-Annotated-GC-Coverage (TAGC) plots of the results from BLAST searches of
638 the NCBI database [84].
639
640 The genome assembly was annotated using the MAKER2 pipeline v2.31 run iteratively in a
641 two-pass fashion (as described in https://github.com/sujaikumar/assemblage/blob/master/
642 README-annotation.md) [85]. Multiple steps are required prior to the first pass though
643 MAKER2 and include creating a repeat library for repeat masking and training three different
644 ab initio gene predictors. Firstly, construction of the repeat library was conducted as
645 described in [86]. In brief, a *de novo* repeat library was created for the assembly by running
646 RepeatModeler v1.0.8 with default parameters, and sequences matching known proteins of
647 repetitive nature were removed from the repeat library through BLASTx against the UniProt

bioRxiv preprint doi: https://doi.org/10.1101/449553; this version posted October 31, 2018. The copyright holder for this preprint (which was not certified by peer review) is the author/funder, who has granted bioRxiv a license to display the preprint in perpetuity. It is made available under aCC-BY 4.0 International license.

database. Next, GeneMark-ES v2.3e was trained on the genome assembly using default parameters with the exception of reducing the –min-contig parameter to 10.000 [87]. SNAP v20131129 and AUGUSTUS v3.0.2 was trained on the genes found by CEGMA and BUSCO, respectively. The generated gene predictors and the repeat library were used in the first pass alongside proteins from UniProt/SwissProt (downloaded 16th February 2016) as protein homology evidence and Mus musculus cDNA as alternative EST evidence (GRCm38 downloaded from Ensembl). For the second pass, SNAP and AUGUSTUS were retrained with the generated MAKER2 predictions and otherwise performed with the same setup. The resulting gene predictions had domain annotations and putative functions added using InterProScan v5.4.47 and BLASTp against the UniProt database with evalue 1e-5 (same methodology as [86,88]). Finally, the output was filtered using the MAKER2 default filtering approach only retaining predictions with AED <1.

Genome mining and gene alignments

We searched for *TLR* genes, associated receptors and adaptor molecules as well as genes of the MHC region (complete list of genes can be found in Additional file 2: Table S4) collected from UniProt and Ensembl. Throughout, we performed tBLASTn searches, manual assembly exon by exon in MEGA7 and verified annotations through reciprocal BLASTx against the NCBI database and phylogenetic analysis including orthologues from human (*Homo sapiens*), mouse (*Mus musculus*), rat (*Rattus norvegicus*) and all three members of the *Gerbillinae* subfamily. For details on the phylogenetic analyses we refer to descriptions in sections below. In the *TLR* analyses Algerian mouse (*M. spretus*), Ryukyu mouse (*M. caroli*), Chinese hamster (*Cricetulus griseus*) and Chinese tree shrew (*Tupaia belangeri chinensis*) were also included.

bioRxiv preprint doi: https://doi.org/10.1101/449553; this version posted October 31, 2018. The copyright holder for this preprint (which was not certified by peer review) is the author/funder, who has granted bioRxiv a license to display the preprint in perpetuity. It is made available under aCC-BY 4.0 International license.

672

673 Sand rat and Mongolian gerbil genome assemblies were downloaded from NCBI (September
674 12th 2017). The genome assemblies of the great gerbil, sand rat and Mongolian gerbil were
675 made into searchable databases for gene mining using the makeblastdb command of the
676 blast+ v2.6.0 program. Local tBLASTn searches, using protein sequences of mouse and
677 occasionally rat, human and Mongolian gerbil as queries, were executed with default
678 parameters including an e-value cut-off of 1e+1. The low e-value was utilized to capture
679 more divergent sequence homologs. Hits were extracted from assemblies using bedtools
680 v2.26.0 and aligned with orthologs in MEGA v7.0.26 using MUSCLE with default parameters.
681 In cases where annotations for some of the *TLRs* for a species were missing in Ensembl and
682 could not be located in either the NCBI nucleotide database or in UniProt, the Ensembl
683 BLAST Tool (tBLASTn) was used with default parameters to find the genomic region of
684 interest using queries from mouse.

685

686 **Synteny analyses of MHC regions**

687 A combination of the Ensembl genome browser v92 and comparisons presented in [89] and
688 tBLASTn searches, as described above, were used in synteny analyses of the MHCI and II
689 regions of human, rat and mouse with great gerbil. Synteny of MHCII genes of sand rat and
690 Mongolian gerbil were also investigated, however for simplicity and visualization purposes
691 not included in the figure (Fig. 3).

692

693 **Alignment and phylogenetic reconstruction of TLR and MHC**

bioRxiv preprint doi: https://doi.org/10.1101/449553; this version posted October 31, 2018. The copyright holder for this preprint (which was not certified by peer review) is the author/funder, who has granted bioRxiv a license to display the preprint in perpetuity. It is made available under aCC-BY 4.0 International license.

694 Sequences were aligned with MAFFT [90] using default parameters: for both nucleotides and
695 amino acid alignments the E-INS-i model was utilized. The resulting alignments were edited
696 manually using Mesquite v3.4 [91]. See Additional file 2: Tables S8-10 for accession numbers.
697
698 Ambiguously aligned characters were removed from each alignment using Gblocks [92] with
699 the least stringent parameters for codons and proteins.
700 Maximum likelihood (ML) phylogenetic analyses were performed using the "AUTO"
701 parameter in RAxML v8.0.26 [93] to establish the evolutionary model with the best fit. The
702 general time reversible (GTR) model was the preferred model for the nucleotide alignments,
703 and JTT for the amino acid alignments. The topology with the highest likelihood score of 100
704 heuristic searches was chosen. Bootstrap values were calculated from 500 pseudoreplicates.
705 Taxa with unstable phylogenetic affinities were pre-filtered using RogueNaRok [94] based on
706 evaluation of a 50 % majority rule (MR) consensus tree, in addition to exclusion of taxa
707 with >50 % gaps in the alignment.
708
709 Bayesian inference (BI) was performed using a modified version of MrBayes v3.2 [95]
710 (https://github.com/astanabe/mrbayes5d). The dataset was executed under a separate
711 gamma distribution. Two independent runs, each with three heated and one cold Markov
712 Chain Monte Carlo (MCMC) chain, were started from a random starting tree. The MCMC
713 chains were run for 20,000,000 generations with trees sampled every 1,000th generation.
714 The posterior probabilities and mean marginal likelihood values of the trees were calculated
715 after the burn-in phase (25 %), which was determined from the marginal likelihood scores of
716 the initially sampled trees. The average split frequencies of the two runs were < 0.01,
717 indicating the convergence of the MCMC chains.

bioRxiv preprint doi: https://doi.org/10.1101/449553; this version posted October 31, 2018. The copyright holder for this preprint (which was not certified by peer review) is the author/funder, who has granted bioRxiv a license to display the preprint in perpetuity. It is made available under aCC-BY 4.0 International license.

Selection analyses

All full-length *TLRs* located in the genomes of great gerbil, sand rat and Mongolian gerbil along with other mammalian *TLRs* (Additional file 2: Table S8) were analysed in both classic Datamonkey and Datamonkey 2.0 (datamonkey.org) testing for signs of selection with a phylogeny guided approach [96,97]. For each *TLR* gene alignment a model test was first run prior to the selection test and the proposed best model was used in the analyses. The mixed effects model of evolution (MEME) and adaptive branch-site random effects model (aBSREL) were used to test for site based and branch level episodic selection, respectively [98-100]. aBSREL was iterated three times per gene alignment, initially running an exploratory analysis were all branches were tested for positive selection and subsequently in a hypothesis mode by which first the Gerbillinae clade and secondly the great gerbil was selected as "foreground" branches to test for positive selection. All *TLR* alignments are available in the Github repository (https://github.com/uio-cels/Nilsson_innate_and_adaptive).

TLR protein structure prediction

Translated full-length great gerbil *TLR* sequences were submitted to the Phyre2 structure prediction server for modelling [101]. All sequences were modelled against human TLR5 (c3j0aA) and the resulting structures were colored for visualization purposes using Jmol (Jmol: an open-source Java viewer for chemical structures in 3D. http://www.jmol.org/). Colors were used to differentiate between helices, sheets and loops as well as the transmembrane domain, linker and TIR domain. Sites found in the MEME selection analysis were indicated in pink and further highlighted with arrows (Additional file

bioRxiv preprint doi: https://doi.org/10.1101/449553; this version posted October 31, 2018. The copyright holder for this preprint (which was not certified by peer review) is the author/funder, who has granted bioRxiv a license to display the preprint in perpetuity. It is made available under aCC-BY 4.0 International license.

741 1: Figures S7-9). All great gerbil PDB files are available in the GitHub repository
742 (https://github.com/uio-cels/Nilsson_innate_and_adaptive).
743
744 As TLR4 is the prototypical PRR for lipopolysaccharide (LPS) which are found in all gram-
745 negative bacteria including *Y. pestis*, we subjected the sequence alignment to additional
746 investigation of certain residues indicated in the literature to have an impact on signaling
747 [19]. These were the residues at position 367 and 434, which in mouse are both basic and
748 positively charged, enabling the mouse TLR4 to maintain some signaling even for
749 hypoacetylated LPS [19]. Hypoacetylated LPS is a common strategy for gram-negative
750 bacteria to avoid recognition and strong stimulation of the TLR4-MD2-CD14 receptor
751 complex [63-65].
752

753 ## MHCII promoter investigation

754 The region 400 bp upstream of human HLA-DRB, mouse H2-Eb and rat RT-Db genes were
755 retrieved from Ensembl (GRch38.p12, GRCm38.p6 and Rnor_6.0). Similarly, the region 400
756 bp upstream of the start codon of DRB genes in the three Gerbillinae were retrieved using
757 bedtools v2.26.0. Putative promoter S-X-Y motifs, as presented for mouse in [102], were
758 manually identified for each gene in MEGA7 and all sequences were subsequently aligned
759 using MUSCLE with default parameters [102].
760

761 ## Peptide binding affinity

762 The functionality of MHCII genes is defined by the degree of expression of the MHC genes
763 themselves, and the proteins ability to bind disease-specific peptides to present to the
764 immune system. The ability of an MHCII protein to bind particular peptides can with some

bioRxiv preprint doi: https://doi.org/10.1101/449553; this version posted October 31, 2018. The copyright holder for this preprint (which was not certified by peer review) is the author/funder, who has granted bioRxiv a license to display the preprint in perpetuity. It is made available under aCC-BY 4.0 International license.

765 degree of confidence be estimated by MHC prediction algorithms, even for unknown MHCII
766 molecules, as long as the alpha and beta-chain protein sequences are available [47]. We
767 here use the NetMHCIIpan predictor v3.2 [47] to estimate the peptide binding affinities of
768 the novel Rhop-DRB3 MHCII molecule and compare it to various other MHCII molecules from
769 great gerbil, mouse, sand rat and Mongolian gerbil. The program was run with default
770 settings and provided with the relevant protein sequences of alpha and beta chains. We
771 compared the predicted binding affinity of these MHCII molecules for 17 known *Y. pestis*
772 epitopes derived from positive ligand assays of *Y. pestis* (https://www.iedb.org/). Specifically,
773 we tested against 16 ligands derived from the F1 capsule antigen of *Y. pestis*, and 1 ligand
774 from the virulence-associated Low calcium V antigen (LcrV) of *Y. pestis*. In addition, we
775 compared the binding affinity of these MHCII molecules against the superantigen *Y.*
776 *pseudotuberculosis* derived mitogen precursor (YPm) [42]. The threshold for binders was set
777 to <500nM [47].
778

779 ## RNA sampling and sequencing

780 Two additional great gerbils were captured in the Midong District outside Urumqi in Xinjiang
781 Province, China, in September 2014. The animals were held in captivity for 35 days before
782 being humanely euthanized and liver tissue samples were conserved in RNA*later*™ at -20 °C
783 prior to RNA extraction. RNA was extracted using standard chloroform procedure [103].
784 Library prep and sequencing were conducted at the Beijing Genomics Institute (BGI,
785 https://www.bgi.com/us/sequencing-services/dna-sequencing/) using Illumina TruSeq RNA
786 Sample Prep Kit and PE sequencing on the HiSeq4000 instrument (150 bp read length).

bioRxiv preprint doi: https://doi.org/10.1101/449553; this version posted October 31, 2018. The copyright holder for this preprint (which was not certified by peer review) is the author/funder, who has granted bioRxiv a license to display the preprint in perpetuity. It is made available under aCC-BY 4.0 International license.

787 The reads were trimmed using trimmomatic v0.36 and mapped to the genome assembly
788 using hisat2 v2.0.5 with default parameters. A raw count matrix was created by using htseq
789 v0.7.2 with default parameters to extract the raw counts from the mapped files.
790

791 ## Acknowledgements

792 All computational work was performed on the Abel Supercomputing Cluster (Norwegian
793 metacenter for High Performance Computing (NOTUR) and the University of Oslo) operated
794 by the Research Computing Services group at USIT, the University of Oslo IT- department
795 and the Cod nodes of CEES. Sequencing library creation and high throughput sequencing was
796 carried out at the Norwegian Sequencing Centre (NSC), University of Oslo, Norway, and
797 McGill University and Genome Quebec Innovation Centre, Canada.
798 We would like to thank Morten Skage for assistance in sequence library construction and Ole
799 K. Tørresen, Srinidhi Varadharajan, Tore O. Elgvin and Cassandra N. Trier for helpful advice
800 and support during assembly and annotations steps of the genome, Helle T. Baalsrud for
801 advice during genome mining and Tone F. Gregers for helpful discussions regarding MHCII.
802 For early access to the sand rat genome assembly we thank John F. Mulley.
803

804 ## Funding

805 This project was funded by University of Oslo Molecular Life Science (MLS, allocation
806 #152950), the Research Council of Norway (RCN grant #179569), the European Research
807 Council (ERC-2012-AdG No. 324249 -MedPlag), the National Natural Science Foundation of
808 China (No. 31430006) and National Key Research & Development Program of China
809 (2016YFC1200100).
810

bioRxiv preprint doi: https://doi.org/10.1101/449553; this version posted October 31, 2018. The copyright holder for this preprint (which was not certified by peer review) is the author/funder, who has granted bioRxiv a license to display the preprint in perpetuity. It is made available under aCC-BY 4.0 International license.

Availability of data and materials

The genome assembly has been deposited at DDBJ/ENA/GenBank under the accession REGO00000000. The version described in this paper is version REGO01000000.

The genome assembly and annotation are also available from FigShare:

In the following GitHub repository are files of immune gene alignments, PDB files and more:

https://github.com/uio-cels/Nilsson_innate_and_adaptive

Authors' contributions

PN created the genome assembly and annotated it, performed all BLAST-based, *TLR* based and promoter analysis and wrote the first draft of the manuscript. MHS conducted the protein model analyses of TLRs and assisted in the BLAST-based and *TLR* analyses. BVS performed the MHCII affinity analyses. RJSO performed phylogenetic analysis of *TLR*, *MHCI* and *MHCII* genes. YZ, sampled, acclimatised and tested individual great gerbil for plague. RL, YC and YS extracted DNA and RNA for sequencing. PN, WRE, BVS, SJ and KSJ designed the sequencing strategy. WRE, BVS, SJ, KSJ, NCS and RY oversaw the project. All authors read and approved the final manuscript.

Ethics approval

Use of great gerbil tissue was approved by the Committee for Animal Welfares of Xinjiang Centre for Disease Control and Prevention, China. Sampling was performed prior to Chinas signature of the Nagoya Protocol (date of accession September 6th 2016). The sampled species have a "least concern" status in the IUCN Red List of Threatened Species.

bioRxiv preprint doi: https://doi.org/10.1101/449553; this version posted October 31, 2018. The copyright holder for this preprint (which was not certified by peer review) is the author/funder, who has granted bioRxiv a license to display the preprint in perpetuity. It is made available under aCC-BY 4.0 International license.

Consent for publication

Not applicable.

Competing interests

The authors declare that they have no competing interests.

Additional files

Additional file 1: Additional figures and one Note detailing the HOX gene mining (DOCX 19.2Mb)

Additional file 2: Additional tables (DOCX 66Kb)

Additional file 3: Peptide binding affinity predictions for all MHCII molecules run in NetMHCIIpan predictor v3.2 (XLSX)

References

1. Anisimov AP, Lindler LE, Pier GB. Intraspecific Diversity of Yersinia pestis. Clinical Microbiology Reviews. 2004;17:434–64.

2. Addink EA, De Jong SM, Davis SA, Dubyanskiy V, Burdelov LA, Leirs H. The use of high-resolution remote sensing for plague surveillance in Kazakhstan. Remote Sensing of Environment. Elsevier; 2010;114:674–81.

3. Nowak RM. Walker's Mammals of the World. JHU Press; 1999.

bioRxiv preprint doi: https://doi.org/10.1101/449553; this version posted October 31, 2018. The copyright holder for this preprint (which was not certified by peer review) is the author/funder, who has granted bioRxiv a license to display the preprint in perpetuity. It is made available under aCC-BY 4.0 International license.

855 4. Zhang Z, Zhong W, Fan N. Rodent problems and management in the grasslands of China.
856 In: Singleton GR, Hinds LA, Krebs CJ, Spratt DM, editors. Rats, mice and people: rodent
857 biology and management. researchgate.net; 2003. pp. 316–9.

858 5. Gage KL, Kosoy MY. Natural history of plague: perspectives from more than a century of
859 research. Annu. Rev. Entomol. 2005;50:505–28.

860 6. Yang R, Anisimov A. *Yersinia pestis*: Retrospective and Perspective. Springer; 2016.

861 7. Stenseth NC, Atshabar BB, Begon M, Belmain SR, Bertherat E, Carniel E, et al. Plague: past,
862 present, and future. PLoS Med. Public Library of Science; 2008;5:e3.

863 8. Bramanti B, Stenseth NC, Walløe L, Lei X. Plague: A Disease Which Changed the Path of
864 Human Civilization. In: Yang R, Anisimov A, editors. *Yersinia pestis*: Retrospective and
865 Perspective. Dordrecht: Springer; 2016. pp. 1–26.

866 9. Hinnebusch BJ, Jarrett CO, Bland DM. "Fleaing" the Plague: Adaptations of Yersinia pestis
867 to Its Insect Vector That Lead to Transmission. Annu. Rev. Microbiol. Annual Reviews;
868 2017;71:215–32.

869 10. Samia NI, Kausrud KL, Heesterbeek H, Ageyev V, Begon M, Chan K-S, et al. Dynamics of
870 the plague–wildlife–human system in Central Asia are controlled by two epidemiological
871 thresholds. Proceedings of the National Academy of Sciences. National Academy of Sciences;
872 2011;108:14527–32.

873 11. Nguyen VK, Parra-Rojas C, Hernandez-Vargas EA. The 2017 plague outbreak in
874 Madagascar: Data descriptions and epidemic modelling. Epidemics. 2018.

bioRxiv preprint doi: https://doi.org/10.1101/449553; this version posted October 31, 2018. The copyright holder for this preprint (which was not certified by peer review) is the author/funder, who has granted bioRxiv a license to display the preprint in perpetuity. It is made available under aCC-BY 4.0 International license.

875 12. Boisier P, Rahalison L, Rasolomaharo M, Ratsitorahina M, Mahafaly M, Razafimahefa M,
876 et al. Epidemiologic Features of Four Successive Annual Outbreaks of Bubonic Plague in
877 Mahajanga, Madagascar. Emerging Infect. Dis. Centers for Disease Control and Prevention;
878 2002;8:311–6.

879 13. Migliani R, Chanteau S, Rahalison L, Ratsitorahina M, Boutin JP, Ratsifasoamanana L, et al.
880 Epidemiological trends for human plague in Madagascar during the second half of the 20th
881 century: a survey of 20 900 notified cases. Tropical Medicine & International Health.
882 Wiley/Blackwell (10.1111); 2006;11:1228–37.

883 14. Rahelinirina S, Rajerison M, Telfer S, Savin C, Carniel E, Duplantier J-M. The Asian house
884 shrew Suncus murinus as a reservoir and source of human outbreaks of plague in
885 Madagascar. Vinetz JM, editor. PLoS Negl Trop Dis. Public Library of Science;
886 2017;11:e0006072.

887 15. Link VB. Plague on the high seas. Public Health Rep. 1951;66:1466–72.

888 16. Sebbane F, Jarrett CO, Gardner D, Long D, Hinnebusch BJ. Role of the Yersinia pestis
889 plasminogen activator in the incidence of distinct septicemic and bubonic forms of flea-
890 borne plague. Proceedings of the National Academy of Sciences. National Acad Sciences;
891 2006;103:5526–30.

892 17. Neefjes J, Jongsma MLM, Paul P, Bakke O. Towards a systems understanding of MHC
893 class I and MHC class II antigen presentation. Nat Rev Immunol. Nature Publishing Group;
894 2011;11:823–36.

895 18. Murphy K, Weaver C. Janeway's Immunobiology, 9th edition. Garland Science; 2016.

bioRxiv preprint doi: https://doi.org/10.1101/449553; this version posted October 31, 2018. The copyright holder for this preprint (which was not certified by peer review) is the author/funder, who has granted bioRxiv a license to display the preprint in perpetuity. It is made available under aCC-BY 4.0 International license.

19. Sironi M, Cagliani R, Forni D, Clerici M. Evolutionary insights into host-pathogen interactions from mammalian sequence data. Nature Publishing Group. Nature Publishing Group; 2015;16:224–36.

20. Brockhurst MA, Chapman T, King KC, Mank JE, Paterson S, Hurst GDD. Running with the Red Queen: the role of biotic conflicts in evolution. Proc. Biol. Sci. 2014;281:20141382–2.

21. Dyer MD, Neff C, Dufford M, Rivera CG, Shattuck D, Bassaganya-Riera J, et al. The human-bacterial pathogen protein interaction networks of Bacillus anthracis, Francisella tularensis, and Yersinia pestis. Rénia L, editor. PLoS ONE. Public Library of Science; 2010;5:e12089.

22. Chung LK, Bliska JB. Yersinia versus host immunity: how a pathogen evades or triggers a protective response. Current Opinion in Microbiology. 2016;29:56–62.

23. Shannon JG, Hasenkrug AM, Dorward DW, Nair V, Carmody AB, Hinnebusch BJ. Yersinia pestis Subverts the Dermal Neutrophil Response in a Mouse Model of Bubonic Plague. mBio. 2013;4:e00170–13–e00170–13.

24. Shannon JG, Bosio CF, Hinnebusch BJ. Dermal Neutrophil, Macrophage and Dendritic Cell Responses to Yersinia pestis Transmitted by Fleas. Monack DM, editor. PLoS Pathog. 2015;11:e1004734.

25. Gonzalez RJ, Lane MC, Wagner NJ, Weening EH, Miller VL. Dissemination of a Highly Virulent Pathogen: Tracking The Early Events That Define Infection. Valdivia RH, editor. PLoS Pathog. 2015;11:e1004587.

bioRxiv preprint doi: https://doi.org/10.1101/449553; this version posted October 31, 2018. The copyright holder for this preprint (which was not certified by peer review) is the author/funder, who has granted bioRxiv a license to display the preprint in perpetuity. It is made available under aCC-BY 4.0 International license.

916 26. Nham T, Filali S, Danne C, Derbise A, Carniel E. Imaging of bubonic plague dynamics by in
917 vivo tracking of bioluminescent Yersinia pestis. PLoS ONE. 2012;7:e34714.

918 27. Yang H, Wang T, Tian G, Zhang Q, Wu X, Xin Y, et al. Host transcriptomic responses to
919 pneumonic plague reveal that Yersinia pestis inhibits both the initial adaptive and innate
920 immune responses in mice. Int. J. Med. Microbiol. 2017;307:64–74.

921 28. Comer JE, Sturdevant DE, Carmody AB, Virtaneva K, Gardner D, Long D, et al.
922 Transcriptomic and innate immune responses to Yersinia pestis in the lymph node during
923 bubonic plague. Infection and Immunity. American Society for Microbiology Journals;
924 2010;78:5086–98.

925 29. Begon M, Klassovskiy N, Ageyev V, Suleimenov B, Atshabar B, Bennett M. Epizootiologic
926 Parameters for Plague in Kazakhstan. Emerging Infect. Dis. Centers for Disease Control and
927 Prevention; 2006;12:268–73.

928 30. Zhang Y, Dai X, Wang X, Maituohuti A, Cui Y, Rehemu A, et al. Dynamics of Yersinia pestis
929 and its antibody response in great gerbils (Rhombomys opimus) by subcutaneous infection.
930 PLoS ONE. 2012;7:e46820.

931 31. Casanova J-L, Abel L. The genetic theory of infectious diseases: a brief history and
932 selected illustrations. Annu Rev Genomics Hum Genet. Annual Reviews; 2013;14:215–43.

933 32. Tollenaere C, Rahalison L, Ranjalahy M, Rahelinirina S, Duplantier JM, Brouat C. CCR5
934 polymorphism and plague resistance in natural populations of the black rat in Madagascar.
935 Infection, Genetics and Evolution. Elsevier; 2008;8:891–7.

bioRxiv preprint doi: https://doi.org/10.1101/449553; this version posted October 31, 2018. The copyright holder for this preprint (which was not certified by peer review) is the author/funder, who has granted bioRxiv a license to display the preprint in perpetuity. It is made available under aCC-BY 4.0 International license.

936 33. Blanchet C, Jaubert J, Carniel E, Fayolle C, Milon G, Szatanik M, et al. Mus spretus
937 SEG/Pas mice resist virulent Yersinia pestis, under multigenic control. Genes and
938 Immunity. Nature Publishing Group; 2010;12:23–30.

939 34. Busch JD, Van Andel R, Cordova J, Colman RE, Keim P, Rocke TE, et al. Population
940 differences in host immune factors may influence survival of Gunnison's prairie dogs
941 (Cynomys gunnisoni) during plague outbreaks. Journal of Wildlife Diseases. 2011;47:968–73.

942 35. Demeure CE, Blanchet C, Fitting C, Fayolle C, Khun H, Szatanik M, et al. Early Systemic
943 Bacterial Dissemination and a Rapid Innate Immune Response Characterize Genetic
944 Resistance to Plague of SEG Mice. Journal of Infectious Diseases. 2011;205:134–43.

945 36. Vladimer GI, Weng D, Paquette SWM, Vanaja SK, Rathinam VAK, Aune MH, et al. The
946 NLRP12 inflammasome recognizes Yersinia pestis. Immunity. 2012;37:96–107.

947 37. Tollenaere C, Jacquet S, Ivanova S, Loiseau A, Duplantier JM, Streiff R, et al. Beyond an
948 AFLP genome scan towards the identification of immune genes involved in plague resistance
949 in Rattus rattus from Madagascar. Mol Ecol. Wiley/Blackwell (10.1111); 2012;22:354–67.

950 38. Busch JD, Van Andel R, Stone NE, Cobble KR, Nottingham R, Lee J, et al. The innate
951 immune response may be important for surviving plague in wild gunnison's prairie dogs.
952 Journal of Wildlife Diseases. 2013;49:920–31.

953 39. Tollenaere C, Ivanova S, Duplantier J-M, Loiseau A, Rahalison L, Rahelinirina S, et al.
954 Contrasted Patterns of Selection on MHC-Linked Microsatellites in Natural Populations of
955 the Malagasy Plague Reservoir. Salamin N, editor. PLoS ONE. Public Library of Science;
956 2012;7:e32814.

bioRxiv preprint doi: https://doi.org/10.1101/449553; this version posted October 31, 2018. The copyright holder for this preprint (which was not certified by peer review) is the author/funder, who has granted bioRxiv a license to display the preprint in perpetuity. It is made available under aCC-BY 4.0 International license.

957 40. Cobble KR, Califf KJ, Stone NE, Shuey MM, Birdsell DN, Colman RE, et al. Genetic variation
958 at the MHC DRB1 locus is similar across Gunnison's prairie dog (Cynomys gunnisoni) colonies
959 regardless of plague history. Ecol Evol. 2016;6:2624–51.

960 41. Bean AGD, Baker ML, Stewart CR, Cowled C, Deffrasnes C, Wang L-F, et al. Studying
961 immunity to zoonotic diseases in the natural host - keeping it real. Nat Rev Immunol. Nature
962 Publishing Group; 2013;13:851–61.

963 42. Monzón-Casanova E, Rudolf R, Starick L, Müller I, Söllner C, Müller N, et al. The Forgotten:
964 Identification and Functional Characterization of MHC Class II Molecules H2-Eb2 and RT1-
965 Db2. J. Immunol. American Association of Immunologists; 2016;196:988–99.

966 43. Ballingall KT, Bontrop RE, Ellis SA, Grimholt U, Hammond JA, Ho C-S, et al. Comparative
967 MHC nomenclature: report from the ISAG/IUIS-VIC committee 2018. Immunogenetics.
968 Springer Berlin Heidelberg; 2018;46:333–8.

969 44. Braunstein NS, Germain RN. The mouse E beta 2 gene: a class II MHC beta gene with
970 limited intraspecies polymorphism and an unusual pattern of transcription. EMBO J.
971 European Molecular Biology Organization; 1986;5:2469–76.

972 45. Kumar S, Stecher G, Tamura K. MEGA7: Molecular Evolutionary Genetics Analysis Version
973 7.0 for Bigger Datasets. Mol. Biol. Evol. 2016;33:1870–4.

974 46. Waterhouse AM, Procter JB, Martin DMA, Clamp M, Barton GJ. Jalview Version 2--a
975 multiple sequence alignment editor and analysis workbench. Bioinformatics. 2009;25:1189–
976 91.

bioRxiv preprint doi: https://doi.org/10.1101/449553; this version posted October 31, 2018. The copyright holder for this preprint (which was not certified by peer review) is the author/funder, who has granted bioRxiv a license to display the preprint in perpetuity. It is made available under aCC-BY 4.0 International license.

977 47. Jensen KK, Andreatta M, Marcatili P, Buus S, Greenbaum JA, Yan Z, et al. Improved
978 methods for predicting peptide binding affinity to MHC class II molecules. Immunology.
979 Wiley/Blackwell (10.1111); 2018;54:159.

980 48. Hargreaves AD, Zhou L, Christensen J, Marletaz F, Liu S, Li F, et al. Genome sequence of a
981 diabetes-prone desert rodent reveals a mutation hotspot around the ParaHox gene cluster.
982 2016;:1–10.

983 49. Kawai T, Akira S. The role of pattern-recognition receptors in innate immunity: update on
984 Toll-like receptors. Nat. Immunol. Nature Publishing Group; 2010;11:373–84.

985 50. Salazar Gonzalez RM, Shehata H, O'Connell MJ, Yang Y, Moreno-Fernandez ME,
986 Chougnet CA, et al. Toxoplasma gondii- derived profilin triggers human toll-like receptor 5-
987 dependent cytokine production. JIN. Karger Publishers; 2014;6:685–94.

988 51. Roach JC, Glusman G, Rowen L, Kaur A, Purcell MK, Smith KD, et al. The evolution of
989 vertebrate Toll-like receptors. Proceedings of the National Academy of Sciences.
990 2005;102:9577–82.

991 52. Temperley ND, Berlin S, Paton IR, Griffin DK, Burt DW. Evolution of the chicken Toll-like
992 receptor gene family: A story of gene gain and gene loss. BMC Genomics 2015 16:1. BioMed
993 Central; 2008;9:62.

994 53. Solbakken MH, Tørresen OK, Nederbragt AJ, Seppola M, Gregers TF, Jakobsen KS, et al.
995 Evolutionary redesign of the Atlantic cod (Gadus morhua L.) Toll-like receptor repertoire by
996 gene losses and expansions. Sci Rep. Nature Publishing Group; 2016;6:39.

bioRxiv preprint doi: https://doi.org/10.1101/449553; this version posted October 31, 2018. The copyright holder for this preprint (which was not certified by peer review) is the author/funder, who has granted bioRxiv a license to display the preprint in perpetuity. It is made available under aCC-BY 4.0 International license.

997 54. Barreiro LB, Ben-Ali M, Quach H, Laval G, Patin E, Pickrell JK, et al. Evolutionary Dynamics
998 of Human Toll-Like Receptors and Their Different Contributions to Host Defense. McVean G,
999 editor. PLOS Genetics. Public Library of Science; 2009;5:e1000562.

1000 55. Babik W, Dudek K, Fijarczyk A, Pabijan M, Stuglik M, Szkotak R, et al. Constraint and
1001 Adaptation in newt Toll-Like Receptor Genes. Genome Biology and Evolution. 2014;7:81–95.

1002 56. Mathur R, Oh H, Zhang D, Park S-G, Seo J, Koblansky A, et al. A Mouse Model of
1003 Salmonella Typhi Infection. Cell. Cell Press; 2012;151:590–602.

1004 57. Oldenburg M, Krüger A, Ferstl R, Kaufmann A, Nees G, Sigmund A, et al. TLR13
1005 Recognizes Bacterial 23S rRNA Devoid of Erythromycin Resistance–Forming Modification.
1006 Science. American Association for the Advancement of Science; 2012;337:1111–5.

1007 58. Chevret P, Dobigny G. Systematics and evolution of the subfamily Gerbillinae (Mammalia,
1008 Rodentia, Muridae). Molecular Phylogenetics and Evolution. Academic Press; 2005;35:674–
1009 88.

1010 59. Dhariwala MO, Olson RM, Anderson DM. Induction of Type I Interferon through a
1011 Noncanonical Toll-Like Receptor 7 Pathway during Yersinia pestis Infection. Bäumler AJ,
1012 editor. Infection and Immunity. 2017;85.

1013 60. Amemiya K, Meyers JL, Rogers TE, Fast RL, Bassett AD, Worsham PL, et al. CpG
1014 oligodeoxynucleotides augment the murine immune response to the Yersinia pestis F1-V
1015 vaccine in bubonic and pneumonic models of plague. Vaccine. 2009;27:2220–9.

bioRxiv preprint doi: https://doi.org/10.1101/449553; this version posted October 31, 2018. The copyright holder for this preprint (which was not certified by peer review) is the author/funder, who has granted bioRxiv a license to display the preprint in perpetuity. It is made available under aCC-BY 4.0 International license.

1016 61. Saikh KU, Kissner TL, Sultana A, Ruthel G, Ulrich RG. Human monocytes infected with
1017 Yersinia pestis express cell surface TLR9 and differentiate into dendritic cells. J. Immunol.
1018 2004;173:7426–34.

1019 62. Celhar T, Pereira-Lopes S, Thornhill SI, Lee HY, Dhillon MK, Poidinger M, et al. TLR7 and
1020 TLR9 ligands regulate antigen presentation by macrophages. Int. Immunol. 2016;28:223–32.

1021 63. Raetz CRH, Reynolds CM, Trent MS, Bishop RE. Lipid A modification systems in gram-
1022 negative bacteria. Annu. Rev. Biochem. Annual Reviews; 2007;76:295–329.

1023 64. Rebeil R, Ernst RK, Gowen BB, Miller SI, Hinnebusch BJ. Variation in lipid A structure in
1024 the pathogenic yersiniae. Mol. Microbiol. Wiley/Blackwell (10.1111); 2004;52:1363–73.

1025 65. Steimle A, Autenrieth IB, Frick J-S. Structure and function: Lipid A modifications in
1026 commensals and pathogens. Int. J. Med. Microbiol. 2016;306:290–301.

1027 66. Foster SL, Medzhitov R. Gene-specific control of the TLR-induced inflammatory response.
1028 Clin. Immunol. 2009;130:7–15.

1029 67. Nei M, Gu X, Sitnikova T. Evolution by the birth-and-death process in multigene families
1030 of the vertebrate immune system. Proceedings of the National Academy of Sciences.
1031 National Academy of Sciences; 1997;94:7799–806.

1032 68. Amadou C, Younger RM, Sims S, Matthews LH, Rogers J, Kumanovics A, et al. Co-
1033 duplication of olfactory receptor and MHC class I genes in the mouse major
1034 histocompatibility complex. Hum. Mol. Genet. 2003;12:3025–40.

bioRxiv preprint doi: https://doi.org/10.1101/449553; this version posted October 31, 2018. The copyright holder for this preprint (which was not certified by peer review) is the author/funder, who has granted bioRxiv a license to display the preprint in perpetuity. It is made available under aCC-BY 4.0 International license.

1035 69. Ohtsuka M, Inoko H, Kulski JK, Yoshimura S. Major histocompatibility complex (Mhc)
1036 class Ib gene duplications, organization and expression patterns in mouse strain C57BL/6.
1037 BMC Genomics 2015 16:1. BioMed Central; 2008;9:178.

1038 70. Hughes AL, Nei M. Evolutionary relationships of class II major-histocompatibility-complex
1039 genes in mammals. Mol. Biol. Evol. 1990;7:491–514.

1040 71. Viļuma A, Mikko S, Hahn D, Skow L, Andersson G, Bergström TF. Genomic structure of
1041 the horse major histocompatibility complex class II region resolved using PacBio long-read
1042 sequencing technology. Sci Rep. Nature Publishing Group; 2017;7:45518.

1043 72. Katju V, Lynch M. The structure and early evolution of recently arisen gene duplicates in
1044 the Caenorhabditis elegans genome. Genetics. Genetics Society of America; 2003;165:1793–
1045 803.

1046 73. Gregers TF, Fleckenstein B, Vartdal F, Roepstorff P, Bakke O, Sandlie I. MHC class II
1047 loading of high or low affinity peptides directed by Ii/peptide fusion constructs: implications
1048 for T cell activation. Int. Immunol. 2003;15:1291–9.

1049 74. Liu X, Zhan Z, Li D, Xu L, Ma F, Zhang P, et al. Intracellular MHC class II molecules promote
1050 TLR-triggered innate immune responses by maintaining activation of the kinase Btk. Nat.
1051 Immunol. Nature Publishing Group; 2011;12:416–24.

1052 75. Matzaraki V, Kumar V, Wijmenga C, Zhernakova A. The MHC locus and genetic
1053 susceptibility to autoimmune and infectious diseases. Genome Biology. BioMed Central;
1054 2017;18:76.

bioRxiv preprint doi: https://doi.org/10.1101/449553; this version posted October 31, 2018. The copyright holder for this preprint (which was not certified by peer review) is the author/funder, who has granted bioRxiv a license to display the preprint in perpetuity. It is made available under aCC-BY 4.0 International license.

1055 76. Zhang Y, Dai X, Wang Q, Chen H, Meng W, Wu K, et al. Transmission efficiency of the
1056 plague pathogen (Y. pestis) by the flea, Xenopsylla skrjabini, to mice and great gerbils.
1057 Parasit Vectors. BioMed Central; 2015;8:256.

1058 77. Martin M. Cutadapt removes adapter sequences from high-throughput sequencing reads.
1059 EMBnet.journal. 2011;17:pp.10–2.

1060 78. Gnerre S, Maccallum I, Przybylski D, Ribeiro FJ, Burton JN, Walker BJ, et al. High-quality
1061 draft assemblies of mammalian genomes from massively parallel sequence data. Proc. Natl.
1062 Acad. Sci. U.S.A. National Acad Sciences; 2011;108:1513–8.

1063 79. Elgvin TO, Trier CN, Tørresen OK, Hagen IJ, Lien S, Nederbragt AJ, et al. The genomic
1064 mosaicism of hybrid speciation. Sci Adv. 2017;3:e1602996.

1065 80. Pujolar JM, Dalén L, Olsen RA, Hansen MM, Madsen J. First de novo whole genome
1066 sequencing and assembly of the pink-footed goose. Genomics. 2018;110:75–9.

1067 81. Parra G, Bradnam K, Korf I. CEGMA: a pipeline to accurately annotate core genes in
1068 eukaryotic genomes. Bioinformatics. 2007;23:1061–7.

1069 82. Parra G, Bradnam K, Ning Z, Keane T, Korf I. Assessing the gene space in draft genomes.
1070 Nucleic Acids Res. 2009;37:289–97.

1071 83. Simão FA, Waterhouse RM, Ioannidis P, Kriventseva EV, Zdobnov EM. BUSCO: assessing
1072 genome assembly and annotation completeness with single-copy orthologs. Bioinformatics.
1073 Oxford University Press; 2015;31:3210–2.

bioRxiv preprint doi: https://doi.org/10.1101/449553; this version posted October 31, 2018. The copyright holder for this preprint (which was not certified by peer review) is the author/funder, who has granted bioRxiv a license to display the preprint in perpetuity. It is made available under aCC-BY 4.0 International license.

1074 84. Kumar S, Jones M, Koutsovoulos G, Clarke M, Blaxter M. Blobology: exploring raw
1075 genome data for contaminants, symbionts and parasites using taxon-annotated GC-coverage
1076 plots. Front Genet. Frontiers; 2013;4:237.

1077 85. Holt C, Yandell M. MAKER2: an annotation pipeline and genome-database management
1078 tool for second-generation genome projects. BMC Bioinformatics. 2011.

1079 86. Varadharajan S, Sandve SR, Gillard GB, Tørresen OK, Mulugeta TD, Hvidsten TR, et al. The
1080 grayling genome reveals selection on gene expression regulation after whole genome
1081 duplication. Genome Biology and Evolution. 2018.

1082 87. Lomsadze A, Ter-Hovhannisyan V, Chernoff YO, Borodovsky M. Gene identification in
1083 novel eukaryotic genomes by self-training algorithm. Nucleic Acids Res. 2005;33:6494–506.

1084 88. Tørresen OK, Brieuc MSO, Solbakken MH, Sørhus E, Nederbragt AJ, Jakobsen KS, et al.
1085 Genomic architecture of haddock (Melanogrammus aeglefinus) shows expansions of innate
1086 immune genes and short tandem repeats. BMC Genomics 2015 16:1. BioMed Central;
1087 2018;19:240.

1088 89. Hurt P, Walter L, Sudbrak R, Klages S, Müller I, Shiina T, et al. The genomic sequence and
1089 comparative analysis of the rat major histocompatibility complex. Genome Res. Cold Spring
1090 Harbor Lab; 2004;14:631–9.

1091 90. Katoh K, Standley DM. MAFFT multiple sequence alignment software version 7:
1092 improvements in performance and usability. Mol. Biol. Evol. 2013;30:772–80.

1093 91. Maddison WP, Maddison DR. Mesquite: a modular system for evolutionary analysis.
1094 Version 3.4.

bioRxiv preprint doi: https://doi.org/10.1101/449553; this version posted October 31, 2018. The copyright holder for this preprint (which was not certified by peer review) is the author/funder, who has granted bioRxiv a license to display the preprint in perpetuity. It is made available under aCC-BY 4.0 International license.

1095 92. Talavera G, Castresana J, Kjer K, Page R, Sullivan J. Improvement of Phylogenies after
1096 Removing Divergent and Ambiguously Aligned Blocks from Protein Sequence Alignments.
1097 Kjer K, Page R, Sullivan J, editors. Systematic Biology. Oxford University Press; 2007;56:564–
1098 77.

1099 93. Stamatakis A. RAxML-VI-HPC: maximum likelihood-based phylogenetic analyses with
1100 thousands of taxa and mixed models. Bioinformatics. Oxford University Press;
1101 2006;22:2688–90.

1102 94. Aberer AJ, Krompass D, Stamatakis A. Pruning rogue taxa improves phylogenetic
1103 accuracy: an efficient algorithm and webservice. Systematic Biology. 2013;62:162–6.

1104 95. Huelsenbeck JP, Ronquist F. MRBAYES: Bayesian inference of phylogenetic trees.
1105 Bioinformatics. 2001;17:754–5.

1106 96. Delport W, Poon AFY, Frost SDW, Kosakovsky Pond SL. Datamonkey 2010: a suite of
1107 phylogenetic analysis tools for evolutionary biology. Bioinformatics. Oxford University Press;
1108 2010;26:2455–7.

1109 97. Weaver S, Shank SD, Spielman SJ, Li M, Muse SV, Kosakovsky Pond SL. Datamonkey 2.0: a
1110 modern web application for characterizing selective and other evolutionary processes. Mol.
1111 Biol. Evol. 2018;83:8916.

1112 98. Kosakovsky Pond SL, Murrell B, Fourment M, Frost SDW, Delport W, Scheffler K. A
1113 Random Effects Branch-Site Model for Detecting Episodic Diversifying Selection. Mol. Biol.
1114 Evol. 2011;28:3033–43.

bioRxiv preprint doi: https://doi.org/10.1101/449553; this version posted October 31, 2018. The copyright holder for this preprint (which was not certified by peer review) is the author/funder, who has granted bioRxiv a license to display the preprint in perpetuity. It is made available under aCC-BY 4.0 International license.

1115 99. Murrell B, Wertheim JO, Moola S, Weighill T, Scheffler K, Kosakovsky Pond SL. Detecting
1116 individual sites subject to episodic diversifying selection. Malik HS, editor. PLOS Genetics.
1117 2012;8:e1002764.

1118 100. Smith MD, Wertheim JO, Weaver S, Murrell B, Scheffler K, Kosakovsky Pond SL. Less is
1119 more: an adaptive branch-site random effects model for efficient detection of episodic
1120 diversifying selection. Mol. Biol. Evol. 2015;32:1342–53.

1121 101. Kelley LA, Mezulis S, Yates CM, Wass MN, Sternberg MJE. The Phyre2 web portal for
1122 protein modeling, prediction and analysis. Nat Protoc. Nature Publishing Group;
1123 2015;10:845–58.

1124 102. Péléraux A, Karlsson L, Chambers J, Peterson PA. Genomic organization of a mouse
1125 MHC class II region including the H2-M and Lmp2 loci. Immunogenetics. 1996;43:204–14.

1126 103. Chomczynski P, Sacchi N. The single-step method of RNA isolation by acid guanidinium
1127 thiocyanate-phenol-chloroform extraction: twenty-something years on. Nat Protoc. Nature
1128 Publishing Group; 2006;1:581–5.